Article

Discovery Medicine 2026; 38(209): 1744–1766
https://doi.org/10.24976/Discov.Med.202638209.136

ETHE1 Orchestrates Metabolic Reprogramming to Drive Lung Cancer Progression and Therapeutic Resistance

Qiannan Song[1], Ye Liu[1], Hua Yan[1], Lijia Zhang[1], Xue Lei[1], Songjiang Liu[2,*]

[1]Graduate School, Heilongjiang University of Chinese Medicine, 150006 Harbin, Heilongjiang, China
[2]Department of Oncology, First Affiliated Hospital, Heilongjiang University of Chinese Medicine, 150006 Harbin, Heilongjiang, China
*Correspondence: 18043599971@163.com (Songjiang Liu)
Submitted: 14 January 2026 Revised: 14 April 2026 Accepted: 22 May 2026 Published: 20 June 2026

Background: Ethylmalonic encephalopathy 1 (ETHE1), a persulfide dioxygenase, is abnormally expressed in various malignancies, but its mechanism and therapeutic potential in lung cancer remain unclear. This study aimed to elucidate the molecular mechanisms through which ETHE1 promotes lung cancer progression via coordination of the PI3K/AKT signaling pathway and tumor metabolism. The feasibility of using ETHE1 as a therapeutic target was also explored.

Methods: Bioinformatics analysis was used to assess ETHE1 expression levels in lung cancer tissues and its relationship with patient prognosis. ETHE1-overexpressing and ETHE1-silenced lung cancer cell models were constructed. CCK-8, BrdU, and Transwell assays were used to detect cell proliferation, migration, and invasion capabilities. Nude mouse lung metastasis models were established to validate the functions of ETHE1 *in vivo*. Western blotting was used to analyze the activation status of the PI3K/AKT signaling pathway. Coexpression analysis and functional enrichment analysis were performed to explore the mechanisms underlying the effects of ETHE1. Molecular docking and cellular experiments were employed to screen potential ETHE1 inhibitors and evaluate their antitumor effects.

Results: ETHE1 was significantly overexpressed in human lung cancer tissues and closely associated with poor patient prognosis. Functional enrichment analysis revealed that genes coexpressed with ETHE1 were involved mainly in cellular metabolism and signal transduction processes. *In vitro* and *in vivo* experiments confirmed that ETHE1 overexpression significantly promoted lung cancer cell proliferation, migration, invasion, and lung metastasis. Mechanistic studies revealed that ETHE1 exerted oncogenic effects by activating the PI3K/AKT signaling pathway. ETHE1 forms a regulatory axis with the key metabolic enzyme hexokinase 2 (HK2), further amplifying its oncogenic effects. ETHE1 silencing significantly enhanced lung cancer cell sensitivity to chemotherapy drugs such as cisplatin and partially reversed drug resistance. Drug screening identified neobavaisoflavone (NBIF) as an effective ETHE1 inhibitor. NBIF treatment suppressed ETHE1 expression and enhanced chemotherapy sensitivity.

Conclusion: ETHE1 plays a crucial role in lung cancer progression by activating the PI3K/AKT signaling pathway and regulating HK2-mediated metabolism. ETHE1 silencing or NBIF inhibition significantly suppressed malignant tumor behaviors and enhanced chemotherapy sensitivity. These findings establish ETHE1 as a promising therapeutic target for lung cancer treatment.

Keywords: ETHE1; lung cancer; neobavaisoflavone; energy metabolism; PI3K/AKT pathway

Introduction

Lung cancer, which is malignant and has the highest cancer mortality rate globally, presents severe challenges to existing therapeutic strategies because of its complex molecular mechanisms and high heterogeneity, with the five-year survival rate for non-small cell lung cancer patients ranging from only 15% to 20% [1,2]. The metabolic reprogramming of tumor cells, which is among the important hallmarks of cancer, provides a rapid energy supply and biosynthetic materials for tumor cells but also maintains the malignant phenotype of tumor cells by regulating signal transduction networks [3,4]. Persulfide dioxygenase 1 (ethylmalonic encephalopathy 1 [ETHE1]) is a mitochondrial sulfide metabolic enzyme that was initially discovered because of its deficiency, which causes ethylmalonic encephalopathy [5]. Under normal physiological conditions, ETHE1 primarily participates in hydrogen sulfide metabolism and the maintenance of intracellular hydrogen sulfide homeostasis [6,7]. However, recent studies have shown that ETHE1 is abnormally overexpressed in various tumors and participates in regulating energy metabolism and signal transduction in tumor cells [8,9]. ETHE1 has been described as a protein capable of shuttling between the nucleus and cytoplasm, inhibiting p53-induced apoptosis by sequestering the transcription factor RELA/NFκB in the cytoplasm and preventing its nuclear accumulation [10]. Additionally, ETHE1 increases p53 acetylation levels by promoting the binding of HDAC1 to p53 [11]. Although it

is an evolutionarily conserved protein, the functional regulation of ETHE1 in lung cancer, particularly the molecular mechanisms through which it affects tumor progression by regulating cellular energy metabolism, requires further investigation.

The PI3K/AKT signaling pathway, one of the most important intracellular growth regulatory pathways, plays a central role in tumorigenesis and development [12–14]. Its abnormal activation promotes tumor cell proliferation and survival but also reshapes the metabolic network of tumor cells by regulating downstream targets. Hexokinase 2 (HK2), a key rate-limiting enzyme in the glycolytic pathway, is overexpressed in various malignant tumors, accelerating glycolysis to provide sufficient energy for tumor cells but also inhibiting apoptosis via mitochondrial binding [15–17]. Increasing evidence indicates that a close regulatory relationship exists between the PI3K/AKT pathway and HK2, resulting in the formation of a "signal–metabolism" regulatory loop that maintains the malignant phenotype of tumors [18]. However, whether ETHE1 affects the energy metabolism and malignant behavior of lung cancer cells by regulating this key axis and the specific molecular basis of this regulatory mechanism remain to be thoroughly investigated.

Natural compounds derived from traditional Chinese medicine (TCM) have consistently been important for new drug development because of their unique structural diversity and excellent biocompatibility [19–21]. Isoflavonoids, an important class of plant secondary metabolites, have extensive biological activities, including antioxidant, anti-inflammatory, and antitumor effects [22]. Neobavaisoflavone (NBIF) is an isoflavonoid isolated from Psoralea corylifolia [23]. Previous studies have demonstrated that NBIF has anti-inflammatory, anticancer, and antioxidant properties [24,25]. Studies have confirmed that NBIF can stimulate osteogenesis by upregulating p38-mediated transcription factor and osteogenic gene expression, suggesting that NBIF may be a potential natural compound for treating bone-related diseases [26]. Although recent studies have shown that NBIF also has certain antitumor activity, its specific mechanisms of action and molecular targets remain unclear, limiting its application potential in tumor therapy. Chemotherapy resistance is the primary cause of lung cancer treatment failure, and drug-resistant tumor cells often exhibit enhanced metabolic activity and energy production capacity, increasing cell survival ability and resistance to the cytotoxic effects of chemotherapy drugs via metabolic reprogramming [27]. Therefore, the development of novel therapeutic agents that can simultaneously interfere with tumor metabolism and reverse chemotherapy resistance holds significant clinical value [28,29]. However, the specific antitumor mechanisms, molecular targets, and ability of NBIF to reverse chemotherapy resistance remain unclear, limiting its application potential in tumor therapy.

On the basis of the aforementioned scientific questions, this study elucidates the key role of the ETHE1-PI3K/AKT-HK2 axis in lung cancer metabolic reprogramming and reveals that NBIF, as a specific inhibitor of ETHE1, can effectively disrupt this malignant regulatory loop. These results demonstrate that ETHE1 is highly expressed in lung cancer tissues and is correlated with poor patient prognosis. ETHE1 upregulates HK2 expression by activating the PI3K/AKT signaling pathway, restoring tumor cell energy metabolism to maintain a malignant phenotype. NBIF inhibits ETHE1 activity via direct binding, suppressing lung cancer cell proliferation, migration, and invasion, ultimately reregulating energy metabolism and enhancing chemotherapy sensitivity.

Methods

ETHE1 Expression Analysis and Prognostic Correlation Analysis in Lung Cancer Tissues

For lung cancer patient data acquisition, RNAseq data from the TCGA-LUAD and TCGA-LUSC projects processed via the STAR pipeline were downloaded and organized from the TCGA database (https://portal.gdc.cancer.gov), and data in TPM format were extracted. The Mann–Whitney U test (Wilcoxon rank sum test) was used to screen for differential expression of ETHE1 between tumor tissues and normal tissues. Kaplan–Meier survival curves were generated for prognostic analysis with the log-rank test. The expression levels of ETHE1 and related genes in human lung cancer tissues and corresponding normal tissues were analyzed on the basis of publicly available data, such as The Human Protein Atlas (THPA) database (https://www.proteinatlas.org/).

Functional Enrichment Analysis of Genes Coexpressed With ETHE1

In this study, transcriptomic data from lung cancer tissues (501 patients total, TCGA-LUSC) with low or high ETHE1 expression levels were analyzed on the basis of the LinkedOmics database (http://linkedomics.org/admin.php). Genes coexpressed with ETHE1 were identified in this study. In particular, a Pearson correlation test was performed to analyze the relationships between ETHE1 transcriptional levels and the expression levels of all other genes across lung cancer tissues. Genes that were significantly correlated ($p < 0.05$) and exhibited a fold change of two or more when high versus low ETHE1 expression groups were compared were selected for further analysis. The Geneedenovo database (https://www.genedenovo.com/) was used to perform enrichment analyses on the basis of the Kyoto Encyclopedia of Genes and Genomes (KEGG) and the Gene Ontology Biological Process (GO BP), Gene Ontology: Cellular Component (GO CC), and Gene Ontology Molecular Function (GO MF) on genes that were differentially expressed between the compared groups.

Cell Culture and Treatment

The cell lines used in this study were obtained from American Type Culture Collection (ATCC). A549 (ATCC® CCL-185™) and H460 (ATCC® HTB-177™) cells were cultured in DMEM (Gibco, 11965092) supplemented with 10% fetal bovine serum (Gibco, 10270-106) at 37 °C in a 5% CO_2 incubator. Prior to experimental use, all the cell lines were routinely authenticated by short tandem repeat (STR) profiling and confirmed to be free of mycoplasma contamination by PCR-based detection methods. The cell supernatants were collected after 24 h of culture for glucose detection, and the cells were subsequently collected for ATP detection. For the gene knockdown experiments, ETHE1 was knocked down using shRNA, while HK2 was knocked down using siRNA. All shRNAs and siRNAs were synthesized by GenePharma (Suzhou, China). The specific shRNA sequences used were ETHE1-shRNA (5′-ccgGATAGACTTTGCTGTTCCAGCttcaagagaGCTGGAACAGCAAAGTCTATCtttttt-3′) and negative control (NC)-shRNA (5′-ccgTTCTCCGAACGTGTCACGTttcaagagaACGTGACACGTTCGGAGAAttttttt-3′). These shRNAs were transfected into lung cancer cell lines using Lipofectamine 3000 transfection reagent (L3000015, Thermo Fisher Scientific). For HK2 knockdown, the siRNA sequence was 5′-GGAGGAUGAAGGUAGAAAUTT-3′, with a nontargeting control siRNA sequence of 5′-UGGUUUACAUGUCGACUAA-3′. HK2 siRNAs were transfected using Lipofectamine RNAiMAX (13778–150, Life Technology). Cells were collected for subsequent analysis 48 h after transfection for all knockdown experiments. For overexpression studies, the target ETHE1 sequence was inserted into the standard pcDNA3.1(+) empty vector (Catalog No. V790-20; Invitrogen, Thermo Fisher Scientific, USA). The resulting custom-synthesized plasmid pcDNA3-ETHE1 and its corresponding control empty plasmid (pcDNA3) were both constructed and purchased from GeneChem (Shanghai, China). The ETHE1 overexpression plasmid contains the full-length human ETHE1 coding sequence (CDS), which is as follows: ccagtcctggaaacagcgcctcgggatgcccagctgatcaaggagctggggctgcggctgctctatgctgtgaatacccactgccacgcggaccacattacaggctcggggctgctccgttccctcctccctggctgccagtctgtcatctcccgccttagtggggcccaggctgacttacacattgaggatggagactccatccgcttcgggcgcttcgcgttggagaccagggccagccctggccacaccccaggctgtgtcaccttcgtcctgaatgaccacagcatggccttcactggagatgccctgttgatccgtgggtgtgggcggacagacttccagcaaggctgtgccaagaccttgtaccactcggtccatgaaaagatcttcacacttccaggagactgtctgatctaccctgctcacgattaccatgggttcacagtgtccaccgtggaggaggagaggactctgaac. Transfection was performed when the cells reached approximately 90% confluence. Plasmids, along with the transfection reagent Lipofectamine, were diluted with Opti-MEM (31985070, Gibco), mixed well, and incubated at room temperature for 5 min; then, the two were mixed together and placed at room temperature for 20 min before being evenly added to six-well plates. The culture medium was changed two days later, and puromycin (Solarbio, P8230) was added as a screening antibiotic at a final concentration of 2 μg/mL. After screening for two weeks, RT–PCR and Western blotting were performed to determine whether ETHE1 was highly expressed at the mRNA and protein levels, ultimately yielding stable high-expression cell lines. For pharmacological interventions, cells were treated with NBIF (10 μM) [24,30,31] or the AKT inhibitor MK-2206 (100 nM) [32] for subsequent *in vitro* experiments. These specific working concentrations were selected on the basis of previous studies and the preliminary viability assays in the current research, ensuring effective target inhibition while minimizing nonspecific off-target cytotoxicity.

Construction of a Cisplatin-Resistant A549 Cell Line (A549-SR)

Cisplatin-resistant A549 cells (A549-SR) were generated by continuously exposing parental A549 cells to progressively increasing concentrations of cisplatin. Parental A549 cells cultured in RPMI-1640 medium supplemented with 10% FBS and 1% penicillin/streptomycin were initially treated with 0.1 μM cisplatin. The cisplatin concentration was gradually increased by 0.1–0.5 μM every two to four weeks, contingent on stable cell growth, until the cells proliferated effectively in 5 μM cisplatin. A549-SR cells were subsequently maintained in medium supplemented with 2.5 μM cisplatin to preserve their resistant phenotype.

Glucose Detection

Cell supernatants were collected and analyzed using a glucose analysis kit (F006-1-1, Nanjing Jiancheng Bioengineering Institute). In accordance with the instructions of the kit, test samples or standards were added to glucose detection reagent and reacted at 37 °C for 10 min. Absorbance values were measured at a wavelength of 505 nm using a microplate reader (Thermo Fisher Scientific, USA).

ATP Detection

Cells were collected and detected using an ATP analysis kit (A095-1-1, Nanjing Jiancheng Bioengineering Institute). In accordance with the instructions of the kit, the cells were homogenized and lysed to collect the supernatants. Substrate solution was mixed with test samples or standards, and the promoter was added and reacted at 37 °C for 30 min. Precipitant was added and mixed thoroughly, and the supernatants were collected for measurement. The absorbance values were measured at a wavelength of 636 nm using a microplate reader. ATP concentrations were calculated according to the standard curve and are expressed as μmol/gprot.

HK2 and G6P Detection

HK2 activity was measured using a Hexokinase Activity Assay Kit (ab136957, Abcam) following the manu-

facturer's protocol. Briefly, cells were harvested and lysed, and the supernatant was collected for the assay. The intracellular glucose-6-phosphate (G6P) concentration was determined using a G6P Assay Kit (ab83426, Abcam) according to the manufacturer's instructions. The absorbances for both assays were read on a microplate reader at the specified wavelengths.

CCK-8 Assay

A CCK-8 kit (CK04 Cell Counting Kit-8, Dojindo Laboratories) was used to determine cell proliferation. The experiments were performed according to the instructions in the kit operation manual. The basic procedure involved seeding cell suspensions (3000 cells per well) in 96-well reaction plates. After 24 h of incubation to allow cell adhesion, 10 µL of CCK-8 solution was added to the culture medium of each well, followed by incubation for 30 min. The absorbance of each sample at 450 nm was measured using a Multiskan FC microplate reader (Thermo Scientific).

5-Bromo-2-Deoxyuridine (BrdU) Incorporation Assay

In accordance with the instructions of the kit (6813, Cell Signaling Technology), the cells were plated in six-well plates at a density of 2×10^5 cells per well. When the cell coverage reached approximately 50%, 10 µmol/L BrdU labeling medium was added, and the cells were cultured in the incubator for 30 min. The six-well plates were removed, the culture medium was discarded, and the cells were fixed. The following day, primary antibody provided by the kit (anti-BrdU antibody) was added and incubated at room temperature for 2 h. After the cells were washed three times with PBS, secondary antibody (Cy3-conjugated red fluorescent antibody, 1:500 dilution) was added and incubated at room temperature for 0.5 h. The cells were subsequently washed three times with PBS, after which the nuclei were counterstained with DAPI (1 µg/mL) for 5 min. Fluorescence was observed, and the cells were photographed using a fluorescence microscope (Olympus, Japan).

Transwell Assay

For the invasion assay, Matrigel (354234, Corning) was preprepared at a 1:8 ratio and plated into Transwell chambers (8 µm pore size; 3422, Corning) overnight. After transfection, the cell suspension was collected, 200 µL of cells were added to the upper chamber, and 750 µL of high-serum culture medium was added to the lower chamber, followed by 24 h of culture. The upper layer of liquid in the chamber was removed, and the cells were sequentially treated with 4% paraformaldehyde and methanol for 20 min each and then stained with crystal violet in the dark for 20 min. The cells were observed under a microscope (Olympus, Japan) and photographed for storage, and the number of stained cells in any 10 random fields was counted. For the migration assay, the Matrigel coating was omitted, and the other steps were the same.

Nude Mouse Lung Metastasis Model

One hundred and eight specific pathogen-free female BALB/c-nu nude mice aged six to eight weeks, each weighing 18–22 g, were purchased from Beijing Vital River Laboratory Animal Technology Co., Ltd. and housed under standard laboratory conditions (12 h light/dark cycle, 22 ± 2 °C, 50% to 60% humidity) with free access to food and water. The mice were acclimatized for one week before the experiments and randomly grouped according to the following experimental requirements (n = 6 mice per group): sh-NC, sh-ETHE1; NC, ETHE1; A549-pcDNA3 + Vehicle, A549-pcDNA3 + MK-2206, A549-ETHE1 + Vehicle, A549-ETHE1 + MK-2206; A549 + DMSO, A549 + NBIF, H460 + DMSO, H460 + NBIF; A549 + DMSO, A549 + cisplatin, A549-cisplatin resistant + DMSO, A549-cisplatin resistant + cisplatin, A549-cisplatin resistant + NBIF, and A549-cisplatin resistant + NBIF + cisplatin groups. Lung cancer cells stably transfected with the empty pcDNA3 plasmid and stably overexpressing ETHE1 were harvested during the logarithmic growth phase, washed two times with PBS, and resuspended in serum-free medium. Approximately 1.0×10^6 cells in a 100 µL volume were injected into the lateral tail vein of each nude mouse using a 27-gauge needle under brief isoflurane anesthesia. Anesthesia was induced with 3% isoflurane and maintained with 1.5% to 2% isoflurane in 100% oxygen, which was administered via a nose cone. The NBIF administration protocol included intraperitoneal injection of 30 mg/kg body weight (NBIF; Catalog No. HY-N0720; MedChemExpress) dissolved in the appropriate vehicle, which was administered once every two days for six weeks starting from the first day post-injection [24]. In the MK-2206 administration protocol, the mice were treated with 50 mg/kg (MK-2206; Catalog No. HY-108232; MedChemExpress) dissolved in the appropriate vehicle once every week starting from the first day post-injection [33]. In the cisplatin administration protocol, the mice were treated with intraperitoneal injections of 6 mg/kg (cisplatin; Catalog No. HY-17394; MedChemExpress) dissolved in sterile saline, which was administered once weekly [33]. The control groups received vehicle only. The body weight and general health status of the mice were monitored two times every week throughout the experiment. After six weeks of treatment, the mice were euthanized by CO_2 asphyxiation followed by cervical dislocation. The lungs were rapidly dissected, gently rinsed with ice-cold PBS to remove blood, and weighed immediately to calculate the lung weight/body weight ratio. Surface metastatic nodules were counted and recorded. Portions of lung tissues were fixed in 4% paraformaldehyde for 24 h at 4 °C for subsequent hematoxylin and eosin (H&E) staining. The remaining lung tissues were snap-frozen in liquid nitrogen and stored at –80 °C for molecular biological detection. In this study, a tail vein injection model of tumor cells was used to investigate lung metastasis, ensuring adherence to ethical standards for animal use. The welfare of all the an-

imals was carefully considered, and their health status was monitored postinjection. Euthanasia procedures were conducted in compliance with the requirements of the Institutional Animal Care and Use Committee of Yi Shengyuan Gene Technology (Tianjin) Co., Ltd. (protocol no. YSY-DWLL-20241515), in accordance with the Guide for the Care and Use of Laboratory Animals, to minimize animal suffering.

H&E Staining

Fixed tissues were dehydrated using a graded ethanol series, cleared in xylene, and embedded in paraffin. Sections (4 µm thick) were then cut, deparaffinized, and rehydrated. After H&E staining, the slides were visualized using an optical microscope (Olympus BX53). For quantitative analysis of lung metastasis, three randomly selected fields per slide were captured at 40× magnification. The total lung area and metastatic tumor area in each image were measured using ImageJ software (National Institutes of Health, USA). The "relative tumor area" was calculated as the ratio of the metastatic tumor area to the total lung area for each field, and the average was used for statistical analysis.

KI-67 Immunofluorescence Staining

After standard dewaxing procedures were performed, lung metastatic foci tissue sections (4 µm thick) were first incubated with 0.1% anti-KI-67 primary antibody (rabbit anti-KI-67, 1:200 dilution; ab15580, Abcam) for 14 h at 4 °C in a constant-humidity environment. After primary antibody incubation, Alexa Fluor Plus 488-labeled donkey anti-rabbit IgG (H+L) (1:1000; A32790, Thermo Fisher, USA) was used for incubation in a humid chamber at room temperature in the dark for 1 h. The cell nuclei were counterstained with DAPI (1 µg/mL; D1306, Invitrogen), and the sections were cover-slipped and observed under fluorescence microscopy, after which the results were recorded. Fluorescence images were captured using a fluorescence microscope (Olympus BX53, Japan) with appropriate filter sets.

Western Blot Detection of PI3K/AKT Phosphorylation

Cells from each group were washed three times with ice-cold PBS and lysed in RIPA buffer (P0013B, Beyotime) supplemented with protease inhibitor cocktail (11697498001, Roche) and phosphatase inhibitor cocktail (04906845001, Roche) on ice for 30 min. The cell lysates were subsequently centrifuged at 12,000 ×g for 15 min at 4 °C, after which the supernatants were collected. The total protein concentration was determined using a BCA protein assay kit (23225, Thermo Fisher Scientific) according to the manufacturer's instructions. Equal amounts of protein (30 µg per lane) were separated by 10% SDS–PAGE and transferred to PVDF membranes (IPVH00010, Millipore) using a wet transfer system at 100 V for 2 h at 4 °C. The membranes were blocked with 5% nonfat milk in TBST (Tris-buffered saline with 0.1% Tween-20) for 1 h at room temperature with gentle shaking. Primary antibodies against ETHE1 (1:1000; ab174302, Abcam), phospho-PI3K (1:1000; AF3242, Affinity), total PI3K (1:1000; 4257, Cell Signaling Technology), phospho-AKT (1:1000, Ser473; 4060, Cell Signaling Technology), total AKT (1:1000; 4691, Cell Signaling Technology), and β-actin (1:5000; A5441, Sigma–Aldrich) were diluted in 5% BSA in TBST and incubated overnight at 4 °C with gentle shaking. After being washed three times with TBST (10 min each), the membranes were incubated with HRP-conjugated secondary antibodies (anti-rabbit IgG, 1:5000; Cell Signaling Technology, 7074; anti-mouse IgG, 1:5000; Cell Signaling Technology, 7076) for 1 h at room temperature. The protein bands were visualized using an enhanced chemiluminescence (ECL) reagent (WBKLS0500, Millipore) and detected by a chemiluminescence imaging system (Bio-Rad ChemiDoc XRS+). Protein expression levels were quantified using ImageJ software, and the phosphorylated protein levels were normalized to their corresponding total protein levels, with β-actin serving as the loading control.

Seahorse Cellular Metabolic Analysis

Cellular bioenergetics were measured using a Seahorse XF96 Extracellular Flux Analyzer (Agilent Technologies, USA) to assess mitochondrial respiration and glycolytic function. Seahorse assays were used to measure the energy metabolism of tumor cells under different treatments, and the metabolic energy levels of ETHE1-overexpressing cell lines were compared. The cells were placed in a 37 °C CO_2 incubator for 1 h, after which the drugs were prepared and diluted to the required concentrations. Diluted drugs were added to the drug ports of the test plate. Cells were sequentially treated with the corresponding drugs at 1 µmol/L each for 1.5 h. Real-time monitoring of the oxygen consumption rate (OCR) and extracellular acidification rate (ECAR) was performed by an XF96 analyzer. Wave software and a report generator were used to analyze the experimental data.

PCR Experiment

Total RNA from cells was extracted and purified using TRIzol reagent (Invitrogen, 15596026, USA). RNA concentration and purity were determined using a NanoDrop 2000 spectrophotometer (Thermo Fisher Scientific, USA). With a PrimeScript RT Reagent Kit (TaKaRa, RR037A, Beijing, China), 1 µg of total RNA from each sample was reverse transcribed to synthesize cDNA, which was subsequently used as an amplification template for gene detection. SYBR Premix Ex Taq Kit (TaKaRa, RR820A, Beijing, China) detection reagent was further used on the Roche LightCycler 480 platform (Roche Diagnostics,

Table 1. Sequences of primers used in this study.

Gene	Forward (5′ → 3′)	Reverse (5′ → 3′)
CCNB1	GGAGAGCATCTAAGATTGGAGAGGTTG	GCTTCGATGTGGCATACTTGTTCTTG
PCNA	GCCGAGATCTCAGCCATATT	ATGTACTTAGAGGTACAAAT
Cyclin A2	AAGAAGCCAGCTGAATCTCAAA	GGTCCAGGTAAACTAATGGCTGAA
Cyclin D1	GCTGCGAAGTGGAAACCATC	CCTCCTTCTGCACACATTTGAA
HK2	TTGACCAGGAGATTGACATGGG	CAACCGCATCAGGACCTCA
ETHE1	GTCATCTCCCGCCTTAGTG	CGGATCAACAGGGCATCT
β-actin	CATGTACGTTGCTATCCAGGC	CTCCTTAATGTCACGCACGAT

Switzerland) for real-time quantitative detection of target genes. The sequences of the primers used are shown in Table 1. The $2^{-\Delta\Delta CT}$ method (β-actin as an internal reference) was used to analyze and compare the relative levels of ETHE1 transcripts between different groups.

Molecular Docking Screening

Molecular docking calculations were performed using Schrödinger Suite 2021-1 (Schrödinger, LLC, New York, NY, USA). The crystal structure of human ETHE1 (PDB ID: 4chl) was downloaded from the RCSB Protein Data Bank. The protein structure was prepared using the Protein Preparation Wizard. Water molecules and heteroatoms were removed. Bond orders were assigned, and missing hydrogen atoms were added. The protonation states of the amino acid residues were generated at pH 7.0 $\pm$ 2.0 using the Epik module. The hydrogen bond network was optimized. Restrained energy minimization was then performed using the OPLS4 force field until the root-mean-square deviation (RMSD) reached 0.3 Å. The TCM compound library was obtained from TCMDatabase@Taiwan [34]. All ligand structures were processed using the LigPrep module. Appropriate tautomers and stereoisomers were generated at physiological pH. The OPLS4 force field was used for ligand energy minimization. The receptor grid box was generated using the receptor grid generation module. The grid box was centered on the active site. The dimensions were set to 20 Å $\times$ 20 Å $\times$ 20 Å to accommodate ligands of various sizes. Virtual screening was executed using the Glide module. A hierarchical docking strategy was applied. First, high-throughput virtual screening (HTVS) was conducted for the initial compound library. The top-ranked compounds were subsequently subjected to standard precision (SP) flexible docking. The ligand flexibility was fully explored during the docking process. The final docking results were evaluated on the basis of the Glide docking score. The binding modes and intermolecular interactions were carefully analyzed.

TUNEL Apoptosis Induction Experiment

Apoptosis was detected using the TdT-mediated dUTP nick end labeling (TUNEL) method with an in situ apoptosis detection kit (Beyotime Biotechnology, Catalog No. C1086, China). Cells were seeded in 24-well plates with coverslips at a density of 5×10^4 cells per well and treated according to the experimental groups. After treatment, the cells were washed two times with PBS and fixed with 4% paraformaldehyde. Staining procedures were performed strictly according to the instructions. DNase I was added as a positive control, and a reaction solution without TdT was added as an NC. After TUNEL staining, the cells were washed three times with PBS and counterstained with DAPI (1 µg/mL; Invitrogen, D1306) for 5 min to visualize the nuclei. Coverslips were mounted using anti-fade mounting medium and examined under a fluorescence microscope (Olympus BX53, Japan) with appropriate filter sets (FITC filter for TUNEL-positive cells: excitation at 488 nm and emission at 530 nm; DAPI filter for nuclei: excitation at 358 nm and emission at 461 nm).

Cell Plate Colony Formation Assay

The transfected cell suspension was diluted to maintain the cell density at approximately 1000 cells per 2 mL, added to 12-well plates, and cultured in a cell culture incubator. The culture medium was changed every four days, and colony formation was observed using a microscope. The upper layer of liquid in the 12-well plates was discarded, and the plates were subsequently washed two times with PBS. The cells were incubated with 4% paraformaldehyde at room temperature for 20 min and then were washed two times with PBS. Crystal violet (C0775; Sigma–Aldrich) staining was performed in the dark for 20 min, after which the cells were washed two times with PBS and air-dried. The colonies were counted macroscopically and photographed using a digital camera.

Statistical Analysis

All the data are presented as the mean $\pm$ standard deviation (SD) from at least three independent experiments, with each experiment performed in triplicate unless otherwise specified. Statistical analyses were performed using GraphPad Prism software (version 9.0; GraphPad Software, Inc., San Diego, CA, USA) and SPSS software (version 26.0; IBM Corp., Armonk, NY, USA). The normality of the data distribution was evaluated via the Shapiro–Wilk test. The homogeneity of variance was assessed via Levene's test. For comparisons between two groups, an unpaired two-tailed Student's *t* test was performed for nor-

mally distributed data, whereas the Mann–Whitney U test was used for nonparametric data. For multiple group comparisons, one-way analysis of variance (ANOVA) followed by Tukey's multiple comparison test was used for parametric data, whereas the Kruskal–Wallis test followed by Dunn's multiple comparison test was applied for nonparametric data. For correlation analyses, the Pearson correlation coefficient was calculated for normally distributed data, while Spearman's rank correlation was used for nonparametric data, including bioinformatics analysis of genes coexpressed with ETHE1. Here, $p < 0.05$ was considered statistically significant.

Results

ETHE1 Expression Is Elevated in Human Lung Cancer and Is Associated With Poor Prognosis

Multiprospective analyses were conducted to identify important functional genes involved in lung cancer development and progression. Genes highly expressed in lung cancer were obtained. With poor prognosis-related genes in lung cancer, tumor mitochondria-related functional genes and oxidative function-related genes were also identified. Venn analysis was performed on these gene sets. The results revealed that ETHE1 and ERO1A were enriched. No studies on ETHE1 related to lung cancer have been reported. Therefore, ETHE1 was selected for subsequent research (Fig. 1a). The expression pattern of ETHE1 in lung cancer was analyzed via bioinformatics approaches to clarify the clinical significance of ETHE1 in lung cancer. Transcriptomic data analysis revealed that ETHE1 mRNA expression levels were higher in lung cancer tissues than in adjacent normal tissues. The protein-level validation results were consistent with these findings. Immunohistochemical staining analysis using the THPA database revealed that the intensity of ETHE1 protein staining in lung cancer tissues was significantly stronger than that in adjacent nontumor tissues (Fig. 1b, $p < 0.01$), confirming that ETHE1 expression is indeed upregulated at both the transcriptional and translational levels in lung cancer. t-SNE dimensionality reduction analysis of single-cell RNA sequencing data revealed that cells with high ETHE1 expression exhibited distinct spatial clustering patterns, suggesting that these cells may possess similar biological characteristics and functional states (Fig. 1c). Clinicopathological feature analysis revealed the important prognostic value of ETHE1 expression. In lung adenocarcinoma patients, ETHE1 expression levels were positively correlated with lymph node metastasis stage (N stage): N0 stage patients (n = 329) had low ETHE1 expression levels, which were not significantly different from those of N1 stage patients (n = 96), whereas N2 stage patients (n = 74) had significantly elevated levels (Fig. 1d, $p < 0.05$), indicating that high ETHE1 expression is closely associated with enhanced tumor metastatic capability. Kaplan–Meier survival analysis based on data obtained from the TCGA database revealed that patients with high ETHE1 expression had shorter overall survival (OS) and progression-free survival (PFS) than those with low ETHE1 expression (Fig. 1e), establishing the clinical value of ETHE1 as a poor prognostic marker for lung cancer. Bioinformatics and clinical data have consistently demonstrated that ETHE1 is highly expressed in human lung cancer, closely associated with the malignant functions of multiple tumors, and serves as an independent risk factor for poor patient prognosis.

ETHE1 Silencing Significantly Inhibits Malignant Behaviors of Lung Cancer Both in Vitro and in Vivo

Genes coexpressed with ETHE1 were analyzed using the LinkedOmics database to understand the biological functions of ETHE1 in lung cancer. Volcano plot analysis revealed extensive correlations between ETHE1 and genome-wide genes, with positively correlated genes being more abundant (**Supplementary Fig. 1a,b**). These findings suggest that ETHE1 functions primarily by activating related genes. GO functional enrichment analysis revealed that genes positively correlated with ETHE1 were significantly enriched in the regulation of cell morphogenesis, positive regulation of cell migration, and regulation of cell motility (**Supplementary Fig. 1c–e**). ETHE1-silenced A549 cell lines were constructed to validate the functional role of ETHE1 in lung cancer progression, and a nude mouse lung metastasis model was established for *in vivo* functional verification. Compared with the control group (sh-NC), the ETHE1-silenced group (sh-ETHE1) exhibited significantly lower lung weight/body weight ratios (Fig. 2a and **Supplementary Fig. 2**; $p < 0.001$). These findings indicate that ETHE1 silencing can reduce pulmonary tumor burden. H&E staining further confirmed that the lung tumor area in the ETHE1-silenced group was markedly smaller than that in the control group (Fig. 2b, $p < 0.001$). These findings demonstrate that ETHE1 silencing inhibited the *in vivo* metastatic capacity of lung cancer cells. The expression of proliferation-related markers in lung metastatic foci was examined to investigate the regulatory effect of ETHE1 on tumor cell proliferation. KI-67 immunofluorescence staining revealed that the percentage of KI-67-positive cells in the ETHE1-silenced group was significantly lower than that in the control group (Fig. 2c; $p < 0.001$). These findings suggest that ETHE1 silencing suppressed tumor cell proliferation. Further molecular mechanism studies revealed that ETHE1 silencing significantly downregulated the mRNA expression of key cell cycle regulatory genes, including Cyclin D1, Cyclin A, Cyclin B1, and PCNA, in lung metastatic foci (Fig. 2d–g, $p < 0.001$). These results indicate that ETHE1 promotes lung cancer cell proliferation by regulating cell cycle progression. *In vitro* functional experiments further validated the above-mentioned findings. CCK-8 proliferation assays demonstrated that ETHE1 silencing significantly inhibited the pro-

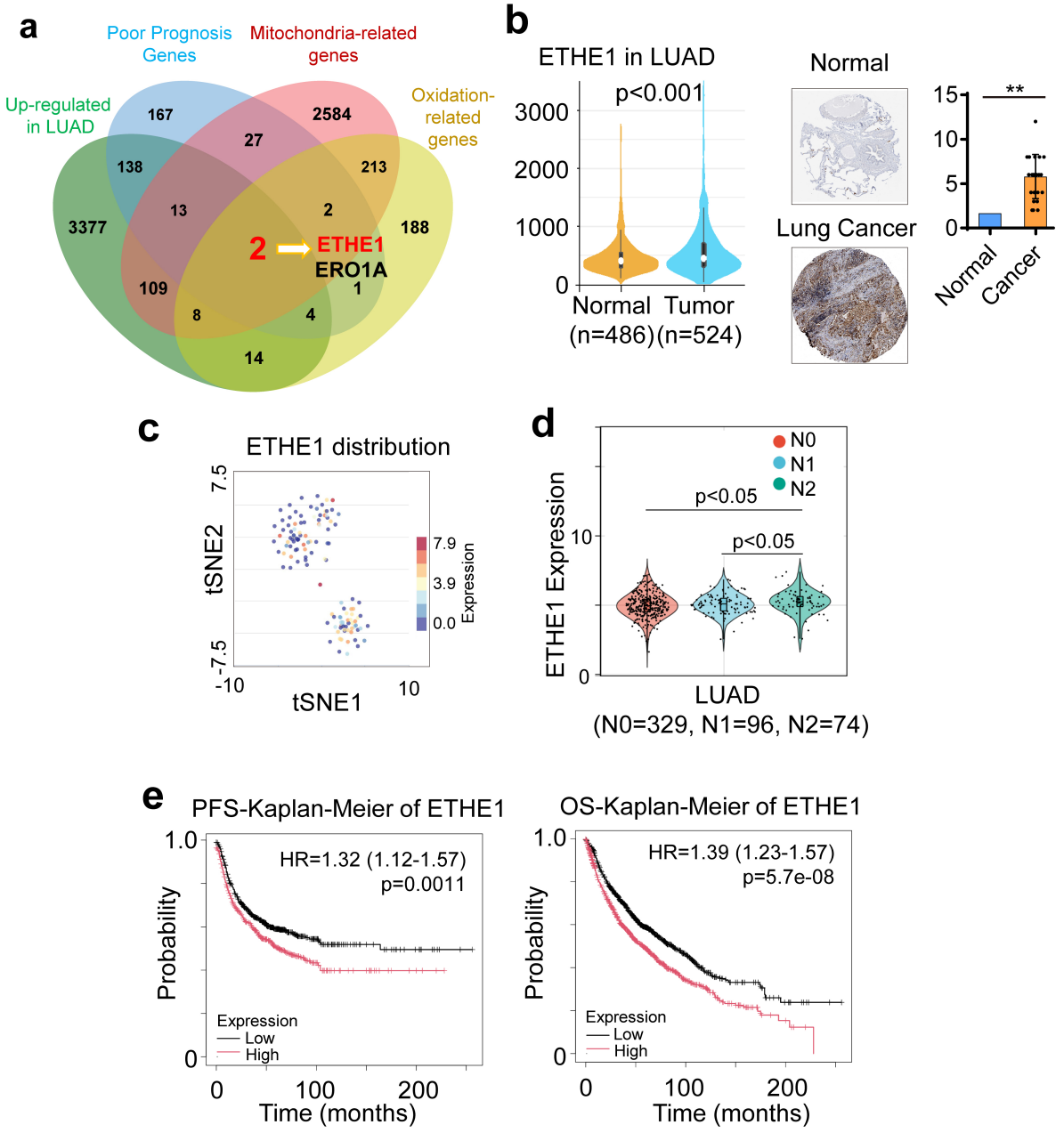

Fig. 1. ETHE1 expression is elevated in human lung cancer and marks tumors with poor prognosis. (a) Venn diagram analysis identifies key functional genes in lung cancer. Four gene sets were analyzed to identify important functional genes in lung cancer development and progression. The gene sets included: highly expressed genes in lung cancer, poor prognosis-related genes in lung cancer, mitochondria-related functional genes, and oxidative function-related genes. The "poor prognosis genes" dataset was obtained from The Human Protein Atlas (https://www.proteinatlas.org/). The "mitochondria-related genes" and "oxidation-related genes" datasets were retrieved from the UniProt database (https://www.uniprot.org/). (b) Data mining analysis showing differential ETHE1 gene expression levels between lung cancer tissues (T, n = 70) and normal lung tissues (N, n = 3) in lung cancer datasets. Expression profiling analysis of ETHE1 protein levels in lung cancer tissues (T) and adjacent non-tumor tissues (N) (patient clinical specimen staining data obtained from The Human Protein Atlas database (https://www.proteinatlas.org/)). (c) t-SNE analysis of single-cell RNA sequencing data showing ETHE1 expression patterns. The single-cell sequencing data were sourced from the CancerSEA database (http://biocc.hrbmu.edu.cn/CancerSEA/). (d) Positive correlation between ETHE1 expression and lymph node metastasis (N staging) in LUAD patients (N0 = 329, N1 = 96, N2 = 74). (e) Kaplan-Meier survival analysis from TCGA lung cancer dataset showing overall survival rates of patients with high versus low intratumoral ETHE1 expression levels (mRNA level). ** $p < 0.01$. ETHE1, ethylmalonic encephalopathy 1; LUAD, lung adenocarcinoma; TCGA, The Cancer Genome Atlas.

liferative activity of both the A549 and H460 lung cancer cell lines (Fig. 2h, $p < 0.05$). The results of the BrdU incorporation experiments were consistent with those of the CCK-8 assays, which revealed that the number of BrdU-positive cells was markedly reduced in the ETHE1-silenced group (Fig. 2i, $p < 0.01$). This finding directly confirms the inhibitory effect of ETHE1 silencing on S-phase cells. Additionally, Transwell migration and invasion assays revealed that ETHE1 silencing significantly reduced both the migration capacity (Fig. 2j, $p < 0.001$) and invasion capacity (Fig. 2k, $p < 0.01$) of A549 and H460 cells. These findings demonstrate that ETHE1 not only regulates tumor cell proliferation but also participates in modulating tumor cell metastatic and invasive properties. Collectively, these results indicate that ETHE1 silencing significantly inhibited lung cancer development and progression by suppressing cell cycle progression, reducing cell proliferation activity, and decreasing tumor cell migration and invasion ability. These findings suggest that ETHE1 may serve as a therapeutic target for lung cancer treatment.

ETHE1 Overexpression Promotes Lung Cancer Initiation and Development

ETHE1-overexpressing A549 lung cancer cell lines were constructed to validate the functional role of ETHE1 in lung cancer progression, and a nude mouse lung metastasis model was established. *In vivo* experiments revealed that six weeks after tail vein injection of ETHE1-overexpressing A549 cells (OE-ETHE1 group), the lung weight/body weight ratio was greater in nude mice than in control mice (OE-NC group), indicating that ETHE1 overexpression promoted increased pulmonary tumor burden (Fig. 3a and **Supplementary Fig. 3**, $p < 0.05$). Histopathological analysis further confirmed that the relative tumor area in the lung tissue of the OE-ETHE1 group of nude mice increased, as shown by H&E staining, which revealed typical tumor cell infiltration and tissue structure destruction (Fig. 3b, $p < 0.001$). Immunofluorescence staining revealed that the proportion of Ki-67-positive cells in lung metastatic foci was greater in the OE-ETHE1 group than in the control group, suggesting that ETHE1 overexpression increased the proliferative activity of tumor cells (Fig. 3c, $p < 0.001$). Molecular-level analysis revealed that ETHE1 overexpression upregulated the mRNA expression of multiple key cell cycle regulatory factors, including Cyclin D1, Cyclin A, Cyclin B1, and PCNA, in lung metastatic foci (Fig. 3d–g, $p < 0.001$). *In vitro* functional experiments further validated the oncogenic role of ETHE1. CCK-8 proliferation assays revealed that ETHE1 overexpression promoted the proliferative capacity of A549 and H460 cells (Fig. 3h, $p < 0.01$). The results of the BrdU incorporation experiments were consistent with these findings, with the proportion of BrdU-positive A549 and H460 cells in the OE-ETHE1 group significantly increasing (Fig. 3i, $p < 0.05$). Tumor metastasis-related functional analysis demonstrated that ETHE1 overexpression enhanced the migration and invasion capabilities of lung cancer cells. Transwell migration assays revealed increased numbers of migrated A549 and H460 cells in the OE-ETHE1 group (Fig. 3j, $p < 0.001$). Transwell invasion assays further confirmed that ETHE1 overexpression enhanced the invasive capacity of A549 and H460 cells (Fig. 3k, $p < 0.05$).

ETHE1 Overexpression Activates Oncogenic PI3K/AKT Signaling

Signaling pathway enrichment analysis was conducted on the basis of the results of previous gene coexpression analyses to elucidate the molecular mechanisms through which ETHE1 exerts its oncogenic effects. The results revealed that genes positively correlated with ETHE1 were enriched in the PI3K signaling pathway (Fig. 4a), suggesting that ETHE1 may exert its biological functions by regulating the PI3K/AKT pathway. This hypothesis was validated by Western blot analysis, and the effects of ETHE1 overexpression on the activity of the PI3K/AKT signaling pathway were evaluated. Compared with the control group, the ETHE1 overexpression group exhibited increased levels of phosphorylated PI3K and AKT (Fig. 4b, $p < 0.001$). Rescue experiments were performed using the AKT-specific inhibitor MK-2206 to further confirm the key role of the PI3K/AKT pathway in the oncogenic functions of ETHE1. BrdU proliferation assays revealed that MK-2206 treatment completely reversed the enhanced cell proliferation caused by ETHE1 overexpression. The number of BrdU-positive cells in the ETHE1 overexpression group was greater than that in the control group, whereas after MK-2206 treatment, the number of BrdU-positive cells in the ETHE1 overexpression group decreased to levels similar to those in the MK-2206-only treatment group (Fig. 4c, $p < 0.01$). Colony formation assays further confirmed these findings, with MK-2206 treatment similarly able to completely block the ability of ETHE1 overexpression to promote long-term cell proliferation (Fig. 4d, $p < 0.001$). Transwell invasion assays revealed that MK-2206 treatment reversed the enhanced cell invasion caused by ETHE1 overexpression, reducing the number of invasive cells to near baseline levels (Fig. 4e, $p < 0.001$). These results indicate that the PI3K/AKT pathway regulates the pro-proliferative effects of ETHE1 but is also key for its pro-invasive effects. Changes in the expression of key cell cycle regulatory proteins were examined to comprehensively explore the role of the PI3K/AKT pathway in the regulation of the cell cycle by ETHE1. The results showed that MK-2206 treatment completely reversed the upregulation of Cyclin D1, Cyclin A, Cyclin B1, and PCNA mRNA expression caused by ETHE1 overexpression (Fig. 4f–i, $p < 0.01$). In the ETHE1 overexpression plus MK-2206 treatment group, the expression levels of these cell cycle proteins decreased to levels similar to those in the MK-2206-only treatment group, indicating that the PI3K/AKT

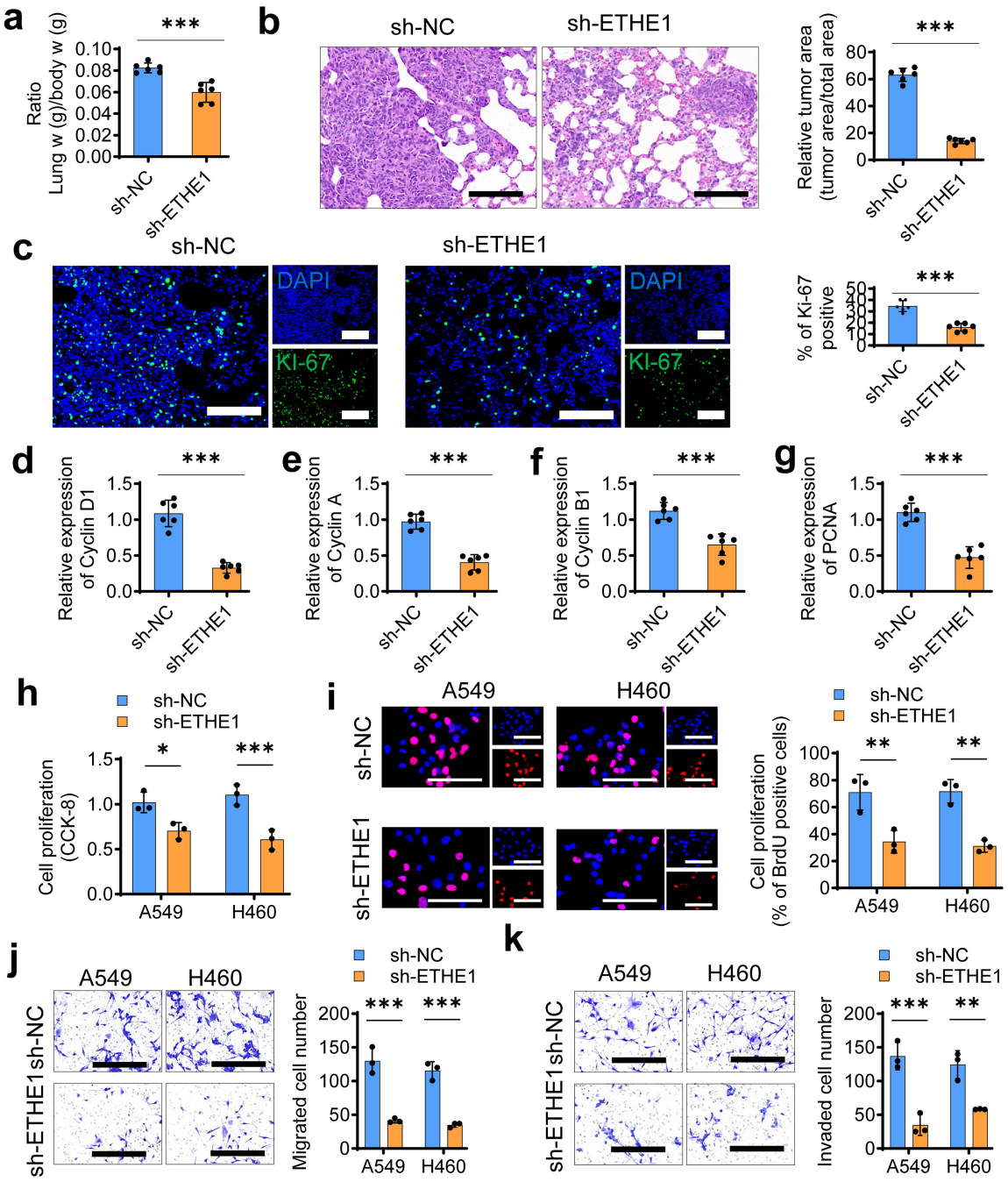

Fig. 2. ETHE1 silencing inhibits lung cancer occurrence and development. (a–c) Nude mice were injected intravenously with A549 lung cancer cells transfected with sh-NC or sh-ETHE1 silencing adenovirus and analyzed after 6 weeks. (a) Lung weight/body weight ratios. (b) H&E staining of lung tissues and quantitative analysis of relative tumor area. n = 6. Scale bar = 200 μm. (c) Representative KI-67 immunostaining and quantitative analysis (n = 6 biologically independent nude mice per group). Scale bar = 200 μm. (d–g) Expression levels of cell cycle-related genes in lung metastatic foci: (d) Cyclin D1, (e) Cyclin A, (f) Cyclin B1, (g) PCNA. (h–k) Effects of ETHE1 silencing on A549 and H460 lung cancer cells: (h) CCK-8 proliferation assay, (i) BrdU proliferation assay, scale bar = 100 μm. (j) Transwell migration assay, scale bar = 100 μm. (k) Transwell invasion assay, scale bar = 100 μm. The data are presented as the means ± SD. n = 3 independent experiments. * $p < 0.05$, ** $p < 0.01$, *** $p < 0.001$. BrdU, 5-Bromo-2-deoxyuridine; SD, standard deviation.

pathway is a key mediator of the regulation of cell cycle progression by ETHE1. The rescue effects of PI3K/AKT pathway inhibition were validated by *in vivo* experiments. Nude mouse tail vein injection experiments revealed that

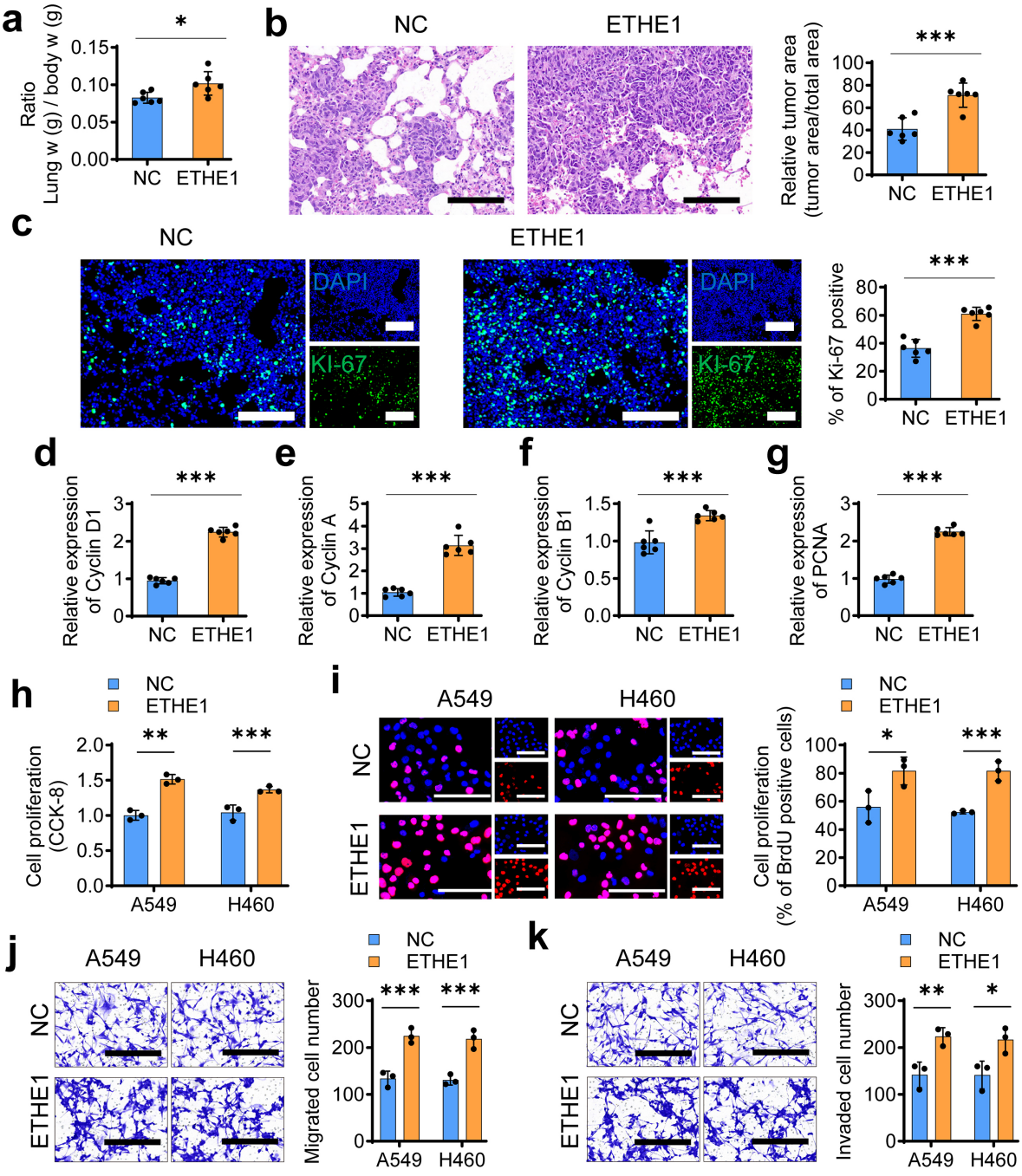

Fig. 3. ETHE1 overexpression promotes lung cancer initiation and progression. (a–c) *In vivo* effects of ETHE1 overexpression in nude mice intravenously injected with A549 cells (OE-NC vs OE-ETHE1, analyzed after 6 weeks, n = 6 per group): (a) Lung weight/body weight ratio, (b) Representative H&E staining and quantitative analysis of relative tumor area. n = 6. Scale bar = 200 μm. (c) Representative Ki-67 immunostaining and quantitative analysis, scale bar = 200 μm. (d–g) Expression levels of cell cycle-related genes in lung metastatic foci: (d) Cyclin D1, (e) Cyclin A, (f) Cyclin B1, (g) PCNA. (h,i) Effects of ETHE1 overexpression on A549 and H460 cell proliferation: (h) CCK-8 assay, (i) BrdU incorporation assay, scale bar = 100 μm. (j,k) Effects of ETHE1 overexpression on A549 and H460 cell motility: (j) Transwell migration assay, scale bar = 100 μm. (k) Transwell invasion assay, scale bar = 100 μm. The data are presented as the means ± SD. n = 3 independent experiments. * $p < 0.05$, ** $p < 0.01$, *** $p < 0.001$.

MK-2206 treatment reduced the relative tumor area formed by ETHE1-overexpressing cells in the lungs (Fig. 4j, $p <$ 0.001). The number of lung metastatic foci in the ETHE1-overexpressing group was significantly greater than that in

the control group, whereas after MK-2206 treatment, the relative tumor area decreased, approaching the level of the MK-2206-only treatment group. These results of the *in vivo* experiment further confirmed the key role of the PI3K/AKT pathway in the prometastatic functions of ETHE1.

HK2 Is Part of an Amplification Loop That Activates and Enhances the Oncogenic Effects of the PI3K/AKT Signaling Pathway on ETHE1

GO functional enrichment analysis was performed on genes coexpressed with ETHE1 to explore the metabolic basis of the oncogenic effects of ETHE1. The results revealed that genes positively correlated with ETHE1 were enriched in glycosyl compound metabolic processes, ATP metabolic processes, and energy derivation by the oxidation of organic compounds (Fig. 5a). Further correlation analysis revealed that the expression of ETHE1 was positively correlated with that of multiple key glycolytic enzyme-encoding genes, with the correlation with HK2 being most prominent (Fig. 5b), suggesting that ETHE1 may influence cellular energy metabolism by regulating HK2. A Seahorse cellular metabolic analyzer was used to detect the effects of ETHE1 overexpression on cellular metabolic activity and ultimately to directly assess the impact of ETHE1 on cellular metabolism. Glycolytic stress test results revealed that ETHE1 overexpression increased the ECAR in A549 cells, indicating enhanced glycolytic activity (Fig. 5c). Conversely, mitochondrial stress tests revealed that ETHE1 overexpression had relatively minimal effects on the OCR (Fig. 5d), suggesting that ETHE1 primarily remodels cellular energy metabolism by promoting glycolysis. These findings are consistent with the Warburg effect, where tumor cells preferentially utilize glycolysis. Changes in cellular glucose uptake capacity were examined to further validate the regulatory role of ETHE1 in glucose metabolism. The results revealed that ETHE1 overexpression increased the cellular glucose uptake rate (Fig. 5e, $p < 0.01$), indicating that ETHE1 can increase the cellular glucose utilization capacity. Moreover, the PCR results revealed that ETHE1 overexpression upregulated HK2 expression (Fig. 5f, $p < 0.001$), which is consistent with the results of the coexpression analysis and further supports the hypothesis that ETHE1 influences glucose metabolism by regulating HK2 expression. HK2 silencing rescue experiments were designed to confirm the key role of HK2 in the regulation of cellular metabolism and oncogenic functions by ETHE1. The silencing efficiency of the siRNA against HK2 was initially validated. The results revealed that si-HK2 treatment reduced HK2 protein expression levels and effectively silenced HK2 expression even in the context of ETHE1 overexpression (Fig. 5g, $p < 0.01$). Similarly, HK2 enzymatic activity assays revealed that HK2 silencing reduced intracellular HK2 catalytic activity and reversed the increase in HK2 activity caused by ETHE1 overexpression (Fig. 5h, $p < 0.01$). Changes in the concentration of the catalytic product of HK2 (i.e., G6P) further confirmed its regulatory effects on HK2 activity. The results revealed that ETHE1 overexpression increased the intracellular G6P concentration, whereas HK2 silencing completely reversed this effect (Fig. 5i, $p < 0.01$), indicating that ETHE1 indeed promotes glucose phosphorylation and the initiation of the glycolytic pathway by upregulating HK2 expression. Functional rescue experiments further confirmed the key role of HK2 in the oncogenic functions of ETHE1. Glucose uptake experiments revealed that HK2 silencing could reduce the glucose uptake capacity of ETHE1-overexpressing cells (Fig. 5j, $p < 0.001$), suggesting that HK2 is an important but not exclusive mechanism through which ETHE1 regulates glucose metabolism. HK2 silencing rescued the oncogenic effects of ETHE1. BrdU proliferation assays revealed that HK2 silencing partially reversed the increase in cell proliferation caused by ETHE1 overexpression (Fig. 5k, $p < 0.001$). The number of BrdU-positive cells in the ETHE1 overexpression group was greater than that in the control group, whereas after HK2 silencing, the number of BrdU-positive cells significantly decreased. Similarly, Transwell invasion assays revealed a similar rescue pattern, with HK2 silencing reducing the invasive capacity of ETHE1-overexpressing cells (Fig. 5l, $p < 0.001$).

ETHE1 Silencing Significantly Enhances Lung Cancer Cell Sensitivity to Cisplatin Chemotherapy

Given the important role of ETHE1 in lung cancer progression, the regulatory mechanism through which ETHE1 affects chemotherapy sensitivity was further investigated. First, the effect of ETHE1 silencing on cisplatin-induced apoptosis was examined. TUNEL staining revealed that in both A549 and H460 cells, cisplatin alone (10 μM, 24 h) [35] or ETHE1 silencing alone could induce moderate apoptosis. However, ETHE1 silencing combined with cisplatin treatment significantly enhanced apoptosis. The number of TUNEL-positive cells was markedly greater than that in the individual treatment groups (Fig. 6a,b; $p < 0.01$). These findings suggest that ETHE1 silencing could enhance the pro-apoptotic effect of cisplatin. Consistent with the apoptosis results, the results of the BrdU incorporation experiments revealed that ETHE1 silencing combined with cisplatin treatment had the most significant inhibitory effect on cell proliferation. In both A549 and H460 cells, the number of BrdU-positive cells in the combination treatment group was significantly lower than that in the control group and individual treatment groups (Fig. 6c,d, $p < 0.01$). These findings indicate that compared with cisplatin, ETHE1 silencing can synergistically suppress tumor cell proliferation, resulting in obvious chemosensitization effects. Cisplatin-resistant A549 cell lines (A549-SR) were established to further validate the role of ETHE1 in chemotherapy resistance, and the effects of different treatment strategies were compared. The results showed that resistant cells exhibited markedly reduced sensitivity to cis-

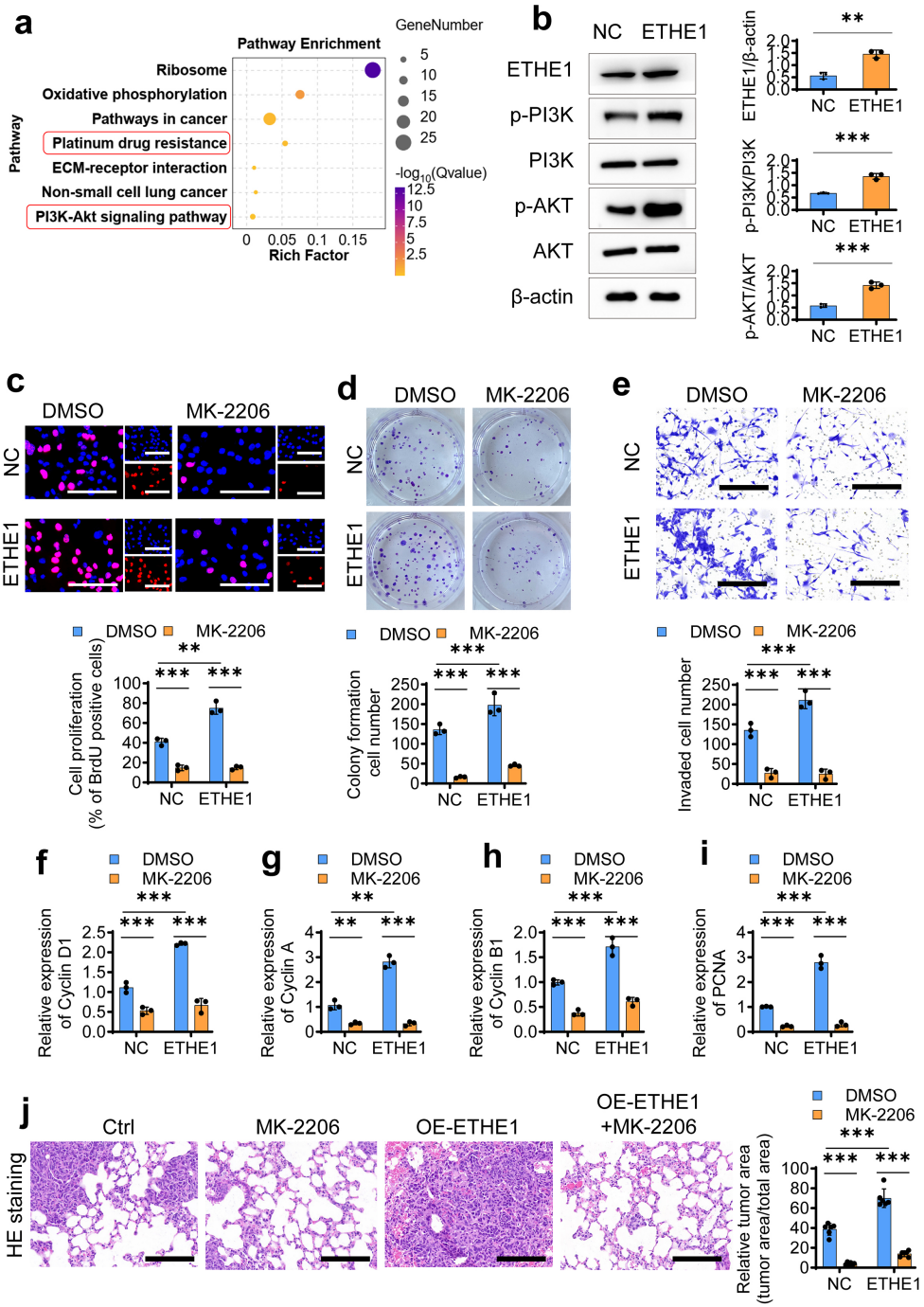

Fig. 4. ETHE1 overexpression activates oncogenic PI3K/AKT signaling pathway. (a) Enrichment analysis of ETHE1 positively co-expressed genes in lung cancer showing upregulation of PI3K pathway and platinum drug resistance functions. (b) Western blot analysis of oncogenic PI3K/AKT pathway alterations in A549 cells with ETHE1 overexpression. (c–e) Effects of PI3K/AKT pathway inhibition (MK-2206, 100 nM, 24 hours) on ETHE1-overexpressing A549 cells: (c) BrdU incorporation assay for proliferation, scale bar = 100 μm. (d) Colony formation assay for proliferation, (e) Transwell invasion assay for invasive capacity, scale bar = 100 μm. (f–i) Expression levels of cell cycle-related genes following PI3K/AKT pathway inhibition: (f) Cyclin D1, (g) Cyclin A, (h) Cyclin B1, (i) PCNA. (j) Nude mouse tail vein injection assay showing that PI3K/AKT pathway inhibition by MK-2206 (50 mg/kg) reverses ETHE1-promoted metastatic capacity. n = 6. Scale bar = 200 μm. The data are presented as the means ± SD. n = 3 independent experiments. ** $p < 0.01$, *** $p < 0.001$.

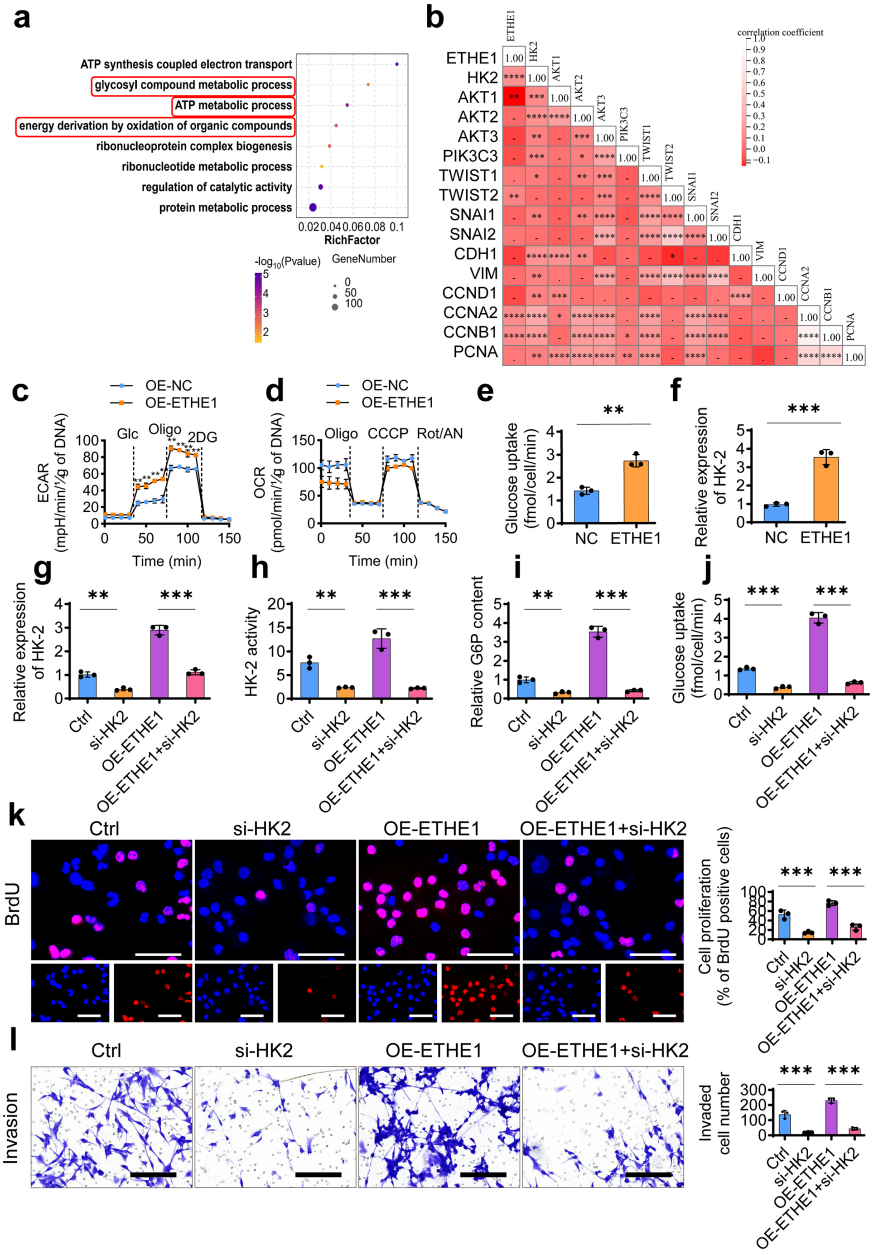

Fig. 5. Hexokinase 2 (HK2) is part of the amplification loop that enhances PI3K/AKT signaling pathway activation in ETHE1-mediated oncogenic effects. (a,b) Bioinformatics analysis: (a) GO enrichment analysis of ETHE1 co-expressed genes showing significant enrichment of energy metabolism and ATP-related functions. (b) Co-expression correlation analysis between ETHE1 and related genes. (c,d) Metabolic profiling in ETHE1-overexpressing A549 cells: (c) Representative extracellular acidification rate (ECAR) traces after glycolytic stress test. (d) Representative oxygen consumption rate (OCR) traces after mitochondrial stress test. Glc, Glucose; Oligo, Oligomycin; 2DG, 2-Deoxy-D-glucose; CCCP, Carbonyl cyanide m-chlorophenyl hydrazone; Rot/AN, Rotenone/Antimycin A. (e,f) Metabolic parameters in ETHE1-overexpressing cells: (e) Glucose uptake rate measurement. (f) Hexokinase 2 (HK2) expression level detection. (g–j) Effects of HK2 silencing on ETHE1-overexpressing cells: (g) HK2 expression level, (h) HK2 activity measurement, (i) Glucose-6-phosphate (G6P) concentration, (j) Glucose uptake rate. (k,l) Functional rescue experiments showing HK2 silencing reverses ETHE1 effects: (k) BrdU incorporation assay for proliferation, scale bar = 100 μm. (l) Transwell invasion assay for invasive capacity, scale bar = 100 μm. The data are presented as the means ± SD. n = 3 independent experiments. * $p < 0.05$, ** $p < 0.01$, *** $p < 0.001$, ****$p < 0.0001$.

platin. The proliferative and invasive capabilities of these cells were significantly greater than those of the parental cells. Notably, ETHE1 silencing partially reversed the resistance phenotype. In resistant cells, the antitumor effect

of ETHE1 silencing combined with cisplatin treatment was comparable to that of cisplatin treatment alone in parental cells (Fig. 6e, $p < 0.01$). In particular, BrdU staining revealed that the proliferative capacity of cells in the combination treatment group (SR + cisplatin + sh-ETHE1) was similar to that in the parental cell cisplatin treatment group (P + cisplatin). Both were significantly lower than those in the other treatment groups among the resistant cells. Similarly, Transwell invasion assays confirmed the abovementioned findings. Resistant cells exhibited stronger invasive capacity. However, compared with cisplatin treatment alone, ETHE1 silencing combined with cisplatin treatment significantly inhibited the invasiveness of resistant cells, reducing their invasive capacity to levels similar to those of the parental cell group (Fig. 6f, $p < 0.01$). These results indicate that ETHE1 not only participates in regulating chemotherapy sensitivity but also affects the metastatic and invasive properties of resistant cells. Collectively, these results demonstrated that ETHE1 silencing significantly increased lung cancer cell sensitivity to chemotherapy by enhancing cisplatin-induced apoptosis, inhibiting tumor cell proliferation, and partially overcoming cisplatin resistance. These findings suggest that ETHE1 may serve as an important therapeutic target for overcoming lung cancer resistance to chemotherapy, providing a new theoretical basis for combination therapy strategies in lung cancer.

ETHE1 Is a Promising Target for Lung Cancer Therapy, and Screening Identified NBIF as a Potential ETHE1-Targeting Inhibitor

ETHE1 was identified as a potential therapeutic target on the basis of the key oncogenic role of ETHE1 in lung cancer established in previous studies, and computer-aided drug design methods were employed to screen for potential ETHE1 inhibitors. Virtual screening based on the structure of the ETHE1 protein revealed high binding scores for NBIF in natural product databases and the lowest binding energy for ETHE1 (Fig. 7a), suggesting that it may be an effective candidate ETHE1 inhibitor. Molecular docking analysis revealed that NBIF could stably bind to the active site of the ETHE1 protein, forming multiple hydrogen bonds and hydrophobic interactions, resulting in favorable binding conformations and interaction patterns (Fig. 7b). The effects of NBIF on lung cancer cell proliferation were evaluated *in vitro* to validate its antitumor activity. The results of the CCK-8 proliferation assay revealed that compared with DMSO treatment, NBIF treatment inhibited the proliferative capacity of A549 and H460 lung cancer cells, with significantly decreased cell viability (Fig. 7c, $p < 0.01$). BrdU incorporation experiments further confirmed these findings, as the number of BrdU-positive cells decreased in both lung cancer cell lines after NBIF treatment (Fig. 7d, $p < 0.001$), indicating that NBIF can effectively inhibit tumor cell DNA synthesis and proliferation processes. Transwell migration assays revealed that compared with control treatment, NBIF treatment reduced the migration capacity of A549 and H460 cells, with the number of cells crossing the chamber membrane significantly lower (Fig. 7e, $p < 0.001$). Similarly, in invasion assays involving Matrigel, NBIF treatment inhibited the invasive capacity of both cell lines (Fig. 7f, $p < 0.001$), indicating that NBIF can inhibit active cell movement but also reduce the cellular capacity to degrade the extracellular matrix. The effects of NBIF on apoptosis were examined to further explore its antitumor mechanisms. TUNEL staining revealed that NBIF treatment could induce apoptosis in A549 and H460 cells, as the number of TUNEL-positive cells significantly increased (Fig. 7g, $p < 0.001$), suggesting that NBIF can inhibit malignant tumor cell behaviors but can also directly induce cell death. The effects of NBIF on key cell cycle regulatory proteins were examined to elucidate the molecular mechanisms underlying its antitumor effects. PCR analysis revealed that NBIF treatment downregulated the mRNA expression levels of Cyclin D1, Cyclin A, Cyclin B1, and PCNA (Fig. 7h–k; $p < 0.001$). Considering the important role of the ETHE1-HK2 regulatory axis in tumor metabolic reprogramming discovered in previous studies, the effects of NBIF on HK2 expression were also examined. The results revealed that NBIF treatment reduced HK2 expression levels (Fig. 7l, $p < 0.01$), which is consistent with the expected effects of an ETHE1 inhibitor and further supports the hypothesis that NBIF functions as an ETHE1 functional inhibitor. The antitumor effects of NBIF were validated by *in vivo* experiments. In a nude mouse lung metastasis model, NBIF treatment reduced the number of pulmonary metastatic foci. H&E staining revealed that compared with that in the lungs of the DMSO control group, the relative tumor area in the lungs of the NBIF-treated group of nude mice was significantly reduced, and the metastatic foci were smaller in volume (Fig. 7m; n = 6 per group; $p < 0.001$). These results from the *in vivo* experiment confirmed that NBIF can effectively inhibit tumor metastasis and growth even in complex *in vivo* environments.

Neobavaisoflavone Enhances Lung Cancer Cell Sensitivity to Chemotherapy Drugs by Modulating ETHE1-Associated Processes

Given that chemotherapy resistance is a major challenge in lung cancer treatment, the role of ETHE1 in the regulation of chemotherapy sensitivity and the potential of NBIF as an ETHE1 inhibitor to reverse chemotherapy resistance were explored. The effect of ETHE1 overexpression on the sensitivity of lung cancer cells to chemotherapy was evaluated. After treatment with 10 μM cisplatin for 24 h, TUNEL apoptosis detection revealed that ETHE1 overexpression reduced the sensitivity of A549 and H460 cells to cisplatin-induced apoptosis. In control cells, cisplatin treatment induced significant apoptosis and markedly increased the number of TUNEL-positive cells; however, in ETHE1-overexpressing cells, the proapoptotic effects of

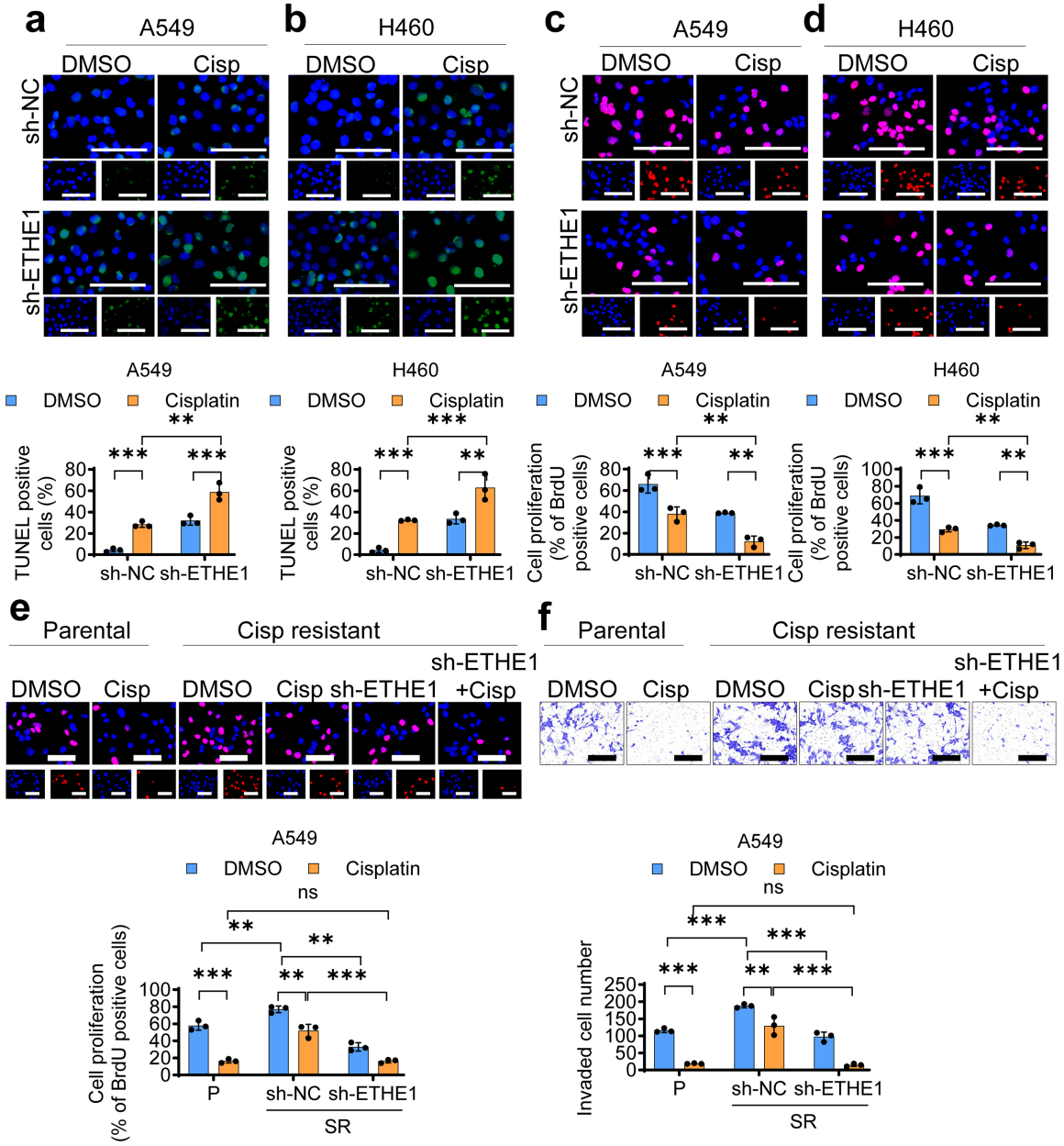

Fig. 6. ETHE1 silencing enhances lung cancer cell sensitivity to chemotherapy drugs. (a,b) TUNEL apoptosis assays in (a) A549 and (b) H460 cells treated with 10 μM cisplatin for 24 hours in sh-NC or ETHE1-silenced cells. Scale bar = 100 μm. (c,d) BrdU proliferation assays in (c) A549 and (d) H460 cells treated with 10 μM cisplatin for 24 hours in sh-NC or ETHE1-silenced cells. Scale bar = 100 μm. (e,f) Effects of cisplatin (10 μM) combined with or without sh-ETHE1 treatment on cisplatin-resistant A549 cells: (e) BrdU proliferation assay, (f) Transwell invasion assay. P (parental), SR (cisplatin-resistant clone). Scale bar = 50 μm. The data are presented as the means ± SD. n = 3 independent experiments. ** $p < 0.01$, *** $p < 0.001$. TUNEL, TdT-mediated dUTP nick end labeling.

cisplatin were significantly attenuated (Fig. 8a,b, $p < 0.05$). Similarly, the results of the BrdU proliferation assay revealed that compared with cisplatin-treated control cells, ETHE1-overexpressing cells maintained increased proliferative activity after cisplatin treatment, with higher numbers of BrdU-positive cells (Fig. 8c,d, $p < 0.01$). These results indicate that ETHE1 overexpression can confer cisplatin resistance to lung cancer cells. Cisplatin-resistant A549 cell lines (SRs) were established to validate the ability of NBIF to reverse chemotherapy resistance. The results of the colony formation assay revealed that cisplatin-resistant cells exhibited obvious resistance to cisplatin treatment, with the colony formation capacity almost unaffected, while the colony formation capacity of parental cells (P) was inhibited by cisplatin. Importantly, NBIF treatment alone effectively inhibited the colony formation capacity

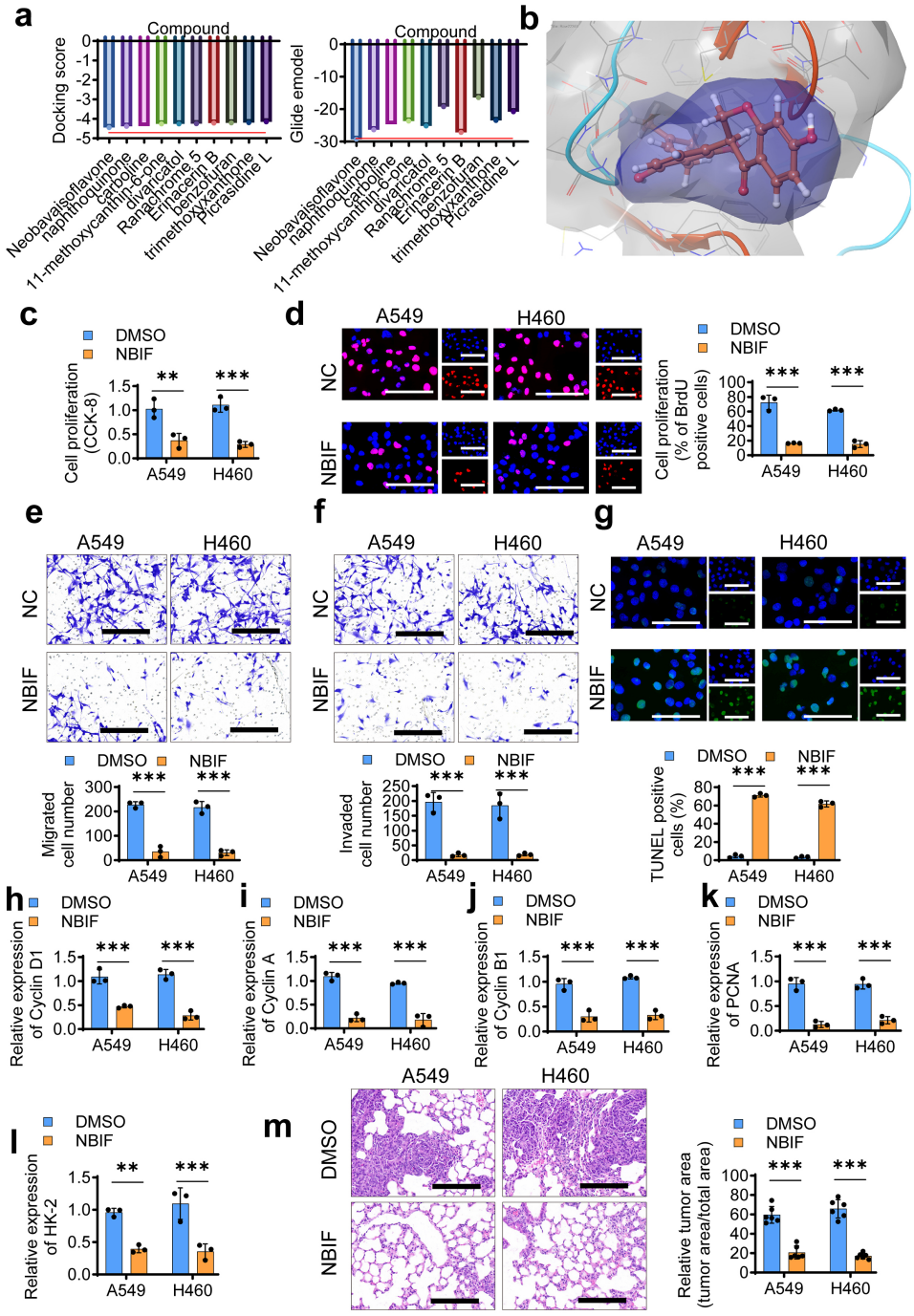

Fig. 7. ETHE1 represents a promising therapeutic target in lung cancer, with screening identifying Neobavaisoflavone (NBIF) as a potential ETHE1-targeting inhibitor. (a,b) Structure-based drug screening against ETHE1: (a) Identification of Neobavaisoflavone with high binding score, (b) Binding conformation display of Neobavaisoflavone with ETHE1. (c,d) Effects of Neobavaisoflavone on A549 and H460 cell proliferation: (c) CCK-8 assay, (d) BrdU incorporation assay. Scale bar = 100 μm. (e,f) Effects of Neobavaisoflavone on A549 and H460 cell motility: (e) Transwell migration assay, (f) Transwell invasion assay. Scale bar = 100 μm. (g) TUNEL assay showing Neobavaisoflavone-induced apoptosis in A549 and H460 cells. Scale bar = 100 μm. (h–k) Expression levels of cell cycle-related genes following Neobavaisoflavone treatment: (h) Cyclin D1, (i) Cyclin A, (j) Cyclin B1, (k) PCNA. (l) Expression level of hexokinase 2 (HK2) following Neobavaisoflavone treatment. (m) Representative H&E staining of nude mouse lung sections and quantitative analysis of relative tumor area (n = 6 biologically independent nude mice per group). Scale bar = 200 μm. The data are presented as the means ± SD. n = 3 independent experiments. ** $p < 0.01$, *** $p < 0.001$.

of resistant cells, and the effect of combined treatment with NBIF and cisplatin was equivalent to that of cisplatin alone on parental cells, indicating that NBIF completely reversed cisplatin resistance (Fig. 8e, $p < 0.01$). BrdU proliferation assays further confirmed the ability of NBIF to reverse resistance. After cisplatin treatment, cisplatin-resistant cells maintained high proliferative activity, while NBIF treatment inhibited the proliferative capacity of resistant cells. The number of BrdU-positive cells in the combination treatment group was similar to that in the parental cells treated with cisplatin alone, again demonstrating that NBIF could effectively restore the antitumor activity of cisplatin (Fig. 8f, $p < 0.01$). *In vivo* experiments further validated the clinical significance of the reversal of chemotherapy resistance by NBIF. In a nude mouse lung metastasis model, cisplatin-resistant cells formed significantly more metastatic foci and were insensitive to cisplatin treatment than parental cells. NBIF treatment reduced the tumor area caused by resistant cells, with the effect of the combination treatment being equivalent to that of cisplatin treatment on sensitive cells (Fig. 8g, $p < 0.05$). These results indicate that NBIF can reverse chemotherapy resistance *in vitro* but is equally effective in complex *in vivo* environments. The cellular glycolytic ATP production levels of NBIF were examined to explore the metabolic mechanisms underlying its ability to reverse chemotherapy resistance. The results revealed that compared with parental cells, cisplatin-resistant cells exhibited higher glycolytic activity with higher ATP production levels, which is consistent with the enhanced metabolic activity of resistant cells. NBIF treatment reduced ATP production levels in resistant cells, whereas the ATP levels in the combination treatment group were similar to those in cisplatin-treated sensitive cells (Fig. 8h, $p < 0.01$). These findings suggest that NBIF may reverse chemotherapy resistance by inhibiting glycolytic metabolism. In all the experiments, the effects of combined NBIF and cisplatin treatment were close to or equivalent to the effects of cisplatin treatment on sensitive cells, indicating that NBIF could completely restore the antitumor activity of cisplatin. Additionally, resistant cells exhibited stronger malignant characteristics across all the parameters (lower apoptosis rates, higher proliferation rates, stronger metastatic capacity, and higher metabolic activity), whereas NBIF treatment effectively reversed these resistance-related malignant phenotypes. Collectively, these results demonstrate that ETHE1 overexpression is among the important mechanisms of lung cancer resistance to chemotherapy and that the use of NBIF as an ETHE1 inhibitor can effectively reverse cisplatin resistance. This reversal involves multiple effects, including restoring the pro-apoptotic effects of chemotherapy drugs, inhibiting the abnormal proliferation and metastatic capacity of resistant cells, and remodeling cellular energy metabolism. These findings reveal the key role of ETHE1 in chemotherapy resistance but also provide important experimental evidence for the clinical application of NBIF as a chemotherapy sensitizer, offering new therapeutic strategies for overcoming lung cancer resistance to chemotherapy (Fig. 9).

Discussion

This study reveals the key role of the persulfide dioxygenase ETHE1 in lung cancer initiation and progression and reveals that NBIF, a specific ETHE1 inhibitor, exerts anti-lung cancer effects by remodeling cellular energy metabolism. These results demonstrate that ETHE1 is highly expressed in human lung cancer tissues and is closely associated with poor patient prognosis, suggesting its potential as an important biomarker for lung cancer diagnosis and prognosis assessment. The results revealed that ETHE1 forms a regulatory axis that promotes lung cancer progression by activating the PI3K/AKT signaling pathway and upregulating HK2 expression, whereas NBIF can specifically inhibit ETHE1 activity, disrupt this malignant regulatory network, and increase lung cancer cell sensitivity to chemotherapy drugs.

ETHE1, a mitochondrial sulfide metabolic enzyme, has rarely been reported for its role in tumors [5]. Bioinformatics analysis and clinical sample validation consistently revealed that ETHE1 expression levels are higher in lung cancer tissues than in normal lung tissues and that high ETHE1 expression is closely associated with poor patient prognosis, shorter OS, and disease-free survival. These findings are consistent with recent research trends regarding the abnormal expression of metabolic enzymes in tumors [36–38]. For example, other key glycolytic enzymes, such as pyruvate kinase M2 and lactate dehydrogenase A, exhibit similar high expression patterns in various tumors [39,40]. Functional enrichment analysis of genes coexpressed with ETHE1 further revealed its close association with pathways related to cellular metabolism, signal transduction, and tumor progression, providing important information for subsequent mechanistic studies. These results collectively indicate that ETHE1 may be an important driver of lung cancer initiation and progression but also a valuable biomarker for predicting patient prognosis. Functional studies confirmed the oncogenic role of ETHE1 in lung cancer progression. ETHE1 overexpression promotes the proliferation, migration, and invasion of lung cancer cells, which echoes the clinical observation of poor prognosis in patients with high ETHE1 expression. The oncogenic effects of ETHE1 are not achieved via a single mechanism but by activating multiple interconnected signaling pathway networks. Activation of the PI3K/AKT pathway, one of the most important intracellular growth regulatory pathways, is a common feature of various tumors. Activation of this pathway directly promotes cell proliferation and antiapoptotic activity but also strongly affects cellular metabolism, growth, and survival by regulating key downstream molecules such as

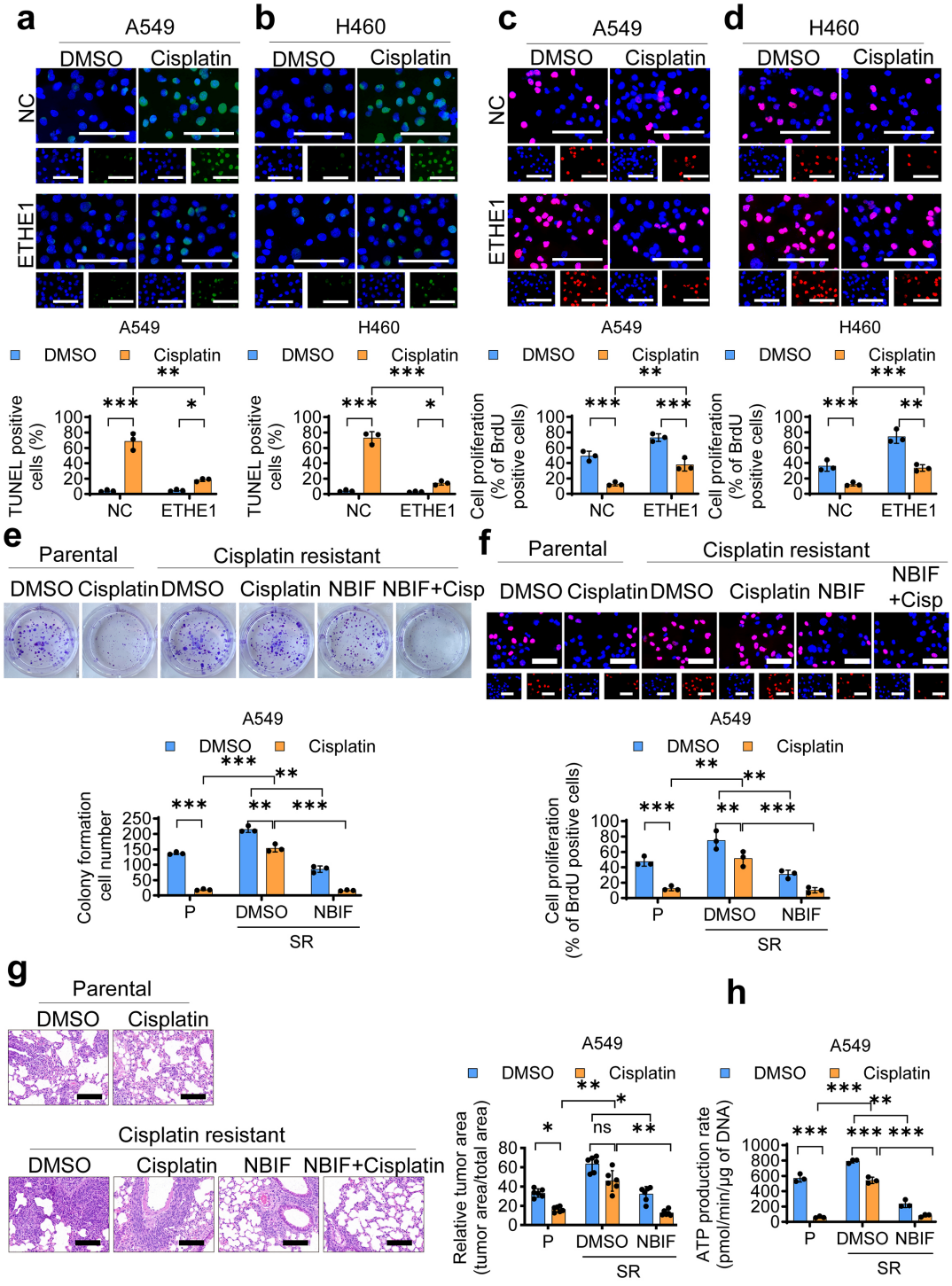

Fig. 8. Neobavaisoflavone modulates ETHE1-associated processes, enhancing lung cancer cell sensitivity to chemotherapy. (a–d) Effects of 10 μM cisplatin treatment for 24 hours in OE-NC or ETHE1-overexpressing cells: (a,b) TUNEL apoptosis assays in A549 and H460 cells respectively, scale bar = 100 μm. (c,d) BrdU proliferation assays in A549 and H460 cells respectively. Scale bar = 100 μm. (e,f) Effects of cisplatin (10 μM) with or without Neobavaisoflavone (10 μM) treatment on cisplatin-resistant A549 cells: (e) Representative colony formation assay, (f) Cell proliferation assay. Scale bar = 100 μm. (g) Neobavaisoflavone inhibits relative tumor area in resistant A549 cell lines. n = 6. Scale bar = 200 μm. (h) ATP production rate from glycolysis in parental or cisplatin-resistant A549 cells. P (parental), SR (cisplatin-resistant clone). The data are presented as the means ± SD. n = 3 independent experiments. ns: not significant, * $p < 0.05$, ** $p < 0.01$, *** $p < 0.001$.

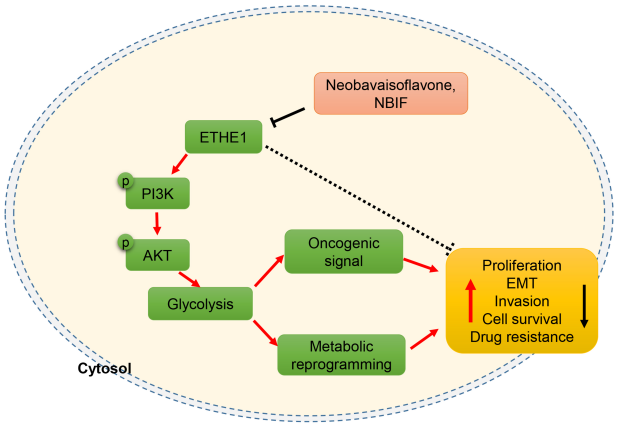

Fig. 9. Overall mechanistic diagram. The role of ETHE1 in lung cancer initiation and progression. ETHE1 activates growth signals (PI3K/AKT signaling pathway), serving as an "oncogenic" factor that tightly connects cellular growth signals (PI3K/AKT signaling pathway) with multiple interconnected metabolic pathways essential for cancer cell growth and proliferation. Neobavaisoflavone, as an ETHE1-targeting inhibitor, exhibits the capacity to suppress lung cancer cells and enhance chemotherapy sensitivity. This figure was drawn by the authors using Microsoft PowerPoint.

mTOR and GSK3β [12,41,42]. Therefore, the discovery that ETHE1 exerts oncogenic effects via PI3K/AKT pathway activation provides an important molecular basis for understanding its function in tumors.

This study also revealed the presence of the ETHE1-PI3K/AKT-HK2 regulatory axis, revealing a new mechanism through which tumor cells maintain their malignant phenotype. HK2, the first rate-limiting enzyme in the glycolytic pathway, is overexpressed as one of the important characteristics of the Warburg effect. ETHE1 upregulates HK2 expression and activity by activating the PI3K/AKT pathway, which amplifies downstream oncogenic effects. This positive feedback mechanism ensures that tumor cells can continuously obtain a sufficient energy supply but also enhances tumor cell survival by inhibiting apoptosis by binding HK2 to mitochondria. The discovery of this regulatory mechanism provides a new perspective for understanding the molecular mechanisms of tumor metabolic reprogramming and explains why targeting the PI3K/AKT pathway or the glycolytic pathway alone often fails to achieve ideal therapeutic effects.

Natural products have consistently been important for new drug development, particularly in the field of cancer therapy [43,44]. Molecular docking screening and experiments validated the ability of NBIF to directly bind to ETHE1 and inhibit its activity, providing important lead compounds for the development of ETHE1-targeted therapeutic agents. NBIF, an isoflavonoid compound isolated from the TCM *Psoralea corylifolia*, is advantageous because of its well-defined structure, abundant sources, and relatively low toxicity and side effects. These results demonstrate that NBIF treatment can inhibit lung cancer cell proliferation, migration, and invasion while reducing PI3K/AKT pathway activity and HK2 expression levels, effectively disrupting the ETHE1-PI3K/AKT-HK2 regulatory axis. These results validate the effectiveness of ETHE1 as a therapeutic target but also demonstrate the therapeutic potential of NBIF as an ETHE1 inhibitor. The finding that NBIF can increase lung cancer cell sensitivity to chemotherapy drugs has important clinical significance. Chemotherapy resistance is among the major challenges in lung cancer treatment, and metabolic reprogramming plays a crucial role in chemotherapy resistance [45]. Drug-resistant tumor cells often exhibit enhanced glycolytic activity and ATP production capacity, which provides more energy for cells to resist the cytotoxicity of chemotherapy drugs but also enhances cellular drug resistance by maintaining the intracellular redox balance and activating survival signals [46]. Inhibiting ETHE1 activity allows NBIF to reregulate tumor cell energy metabolism and reduce tumor cell dependence on glycolysis, thereby weakening cellular drug resistance. This "metabolic resensitization" strategy provides new insights for reversing chemotherapy resistance and establishes a theoretical foundation for the application of NBIF in lung cancer combination therapy.

From a clinical translation perspective, the findings of this study have important application value. First, ETHE1 can serve as a diagnostic marker and prognostic indicator for lung cancer, and detecting ETHE1 expression levels in patient tumor tissues or blood can aid in early disease diagnosis and prognosis assessment. Second, the use of ETHE1 as a therapeutic target provides new options for the precise treatment of lung cancer, particularly for patient subgroups with high ETHE1 expression. Third, NBIF, as a naturally derived ETHE1 inhibitor, has a good druggability foundation and is expected to be developed into a new anti-lung cancer drug via further structural optimization and pharmacological studies. Finally, the combined application strategy of NBIF with traditional chemotherapy drugs provides new possibilities for improving the efficacy of lung cancer treatment, reducing the dosage of chemotherapy, and minimizing toxic side effects.

However, this study still has certain limitations. Although the existence of the ETHE1-PI3K/AKT-HK2 regulatory axis has been validated by various cellular and molecular biological methods, the specific underlying molecular mechanisms still require further in-depth investigation. For example, questions such as how ETHE1 directly or indirectly activates the PI3K/AKT pathway and whether other intermediate regulatory molecules exist remain to be answered. This research is primarily based on *in vitro* cell experiments, which, while having good controllability and reproducibility, may be affected by the complexity of the *in vivo* tumor microenvironment in terms of the actual therapeutic effects of NBIF. Therefore, more animal model stud-

ies and preclinical evaluations are needed to validate its safety and efficacy.

Conclusion

Overall, the results of this study reveal the important role of ETHE1 in lung cancer and its molecular mechanisms in regulating cellular energy metabolism, revealing the antitumor activity of NBIF as an ETHE1 inhibitor and its potential for reversing chemotherapy resistance. These findings not only increase the understanding of lung cancer pathogenesis but also provide important theoretical foundations and experimental evidence for the development of new lung cancer diagnostic and therapeutic strategies.

Availability of Data and Materials

All data generated or analyzed during this study are included in this published article and its supplementary information files. Specific datasets referenced in the Methods section include: Transcriptomic Data: RNA-seq data from The Cancer Genome Atlas (TCGA) for lung adenocarcinoma (TCGA-LUAD) and lung squamous cell carcinoma (TCGA-LUSC), specifically utilizing expression data in TPM format obtained via the GDC data repository. The links for the specific datasets are as follows: TCGA-LUAD: https://portal.gdc.cancer.gov/projects/TCGA-LUAD; TCGA-LUSC: https://portal.gdc.cancer.gov/projects/TCGA-LUSC. Co-expression Analysis: Data analyses were performed using the LinkedOmics database, focusing on the TCGA-LUSC cohort with 501 cases analyzed. The direct link to LinkedOmics is: https://www.linkedomics.org/admin.php. Structural Data: The structural data related to ETHE1 were referenced from the RCSB Protein Data Bank (PDB ID: 4CHL). The direct link to the PDB entry is: https://www.rcsb.org/structure/4CHL.

Author Contributions

SL conceived and designed the study; QS, HY, LZ, YL and XL performed cellular experiments; QS performed animal experiment; QS, HY, YL and XL conducted statistical analysis, QS and SL wrote the manuscript. All authors reviewed the manuscript and critically revised it for important intellectual content. All authors read and approved the final manuscript. All authors agreed to be accountable for all aspects of the work in ensuring that questions related to the accuracy or integrity of any part of the work are appropriately investigated and resolved.

Ethics Approval and Consent to Participate

All the animal experiments were complied with the guidelines of the Medical Experimental Animal Care and ARRIVE guidelines 2.0, and animal protocols were approved by the Institutional Animal Care and Use Committee of Yi Shengyuan Gene Technology (Tianjin) Co., Ltd. (protocol number YSY-DWLL-20241702).

Acknowledgment

Not applicable.

Funding

This work was supported by the National Masters of Traditional Chinese Medicine Academic Thought Inheritance Research Project (Grant No. GY2022-05) and The National Natural Science Foundation of China (Grant No. PYMS202501004).

Conflict of Interest

The authors declare no conflict of interest.

Supplementary Material

Supplementary material associated with this article can be found, in the online version, at https://doi.org/10.24976/Discov.Med.202638209.136.

References

[1] Hill W, Lim EL, Weeden CE, Lee C, Augustine M, Chen K, *et al*. Lung adenocarcinoma promotion by air pollutants. Nature. 2023; 616: 159–167. https://doi.org/10.1038/s41586-023-05874-3.

[2] Karasaki T, Moore DA, Veeriah S, Naceur-Lombardelli C, Toncheva A, Magno N, *et al*. Evolutionary characterization of lung adenocarcinoma morphology in TRACERx. Nature Medicine. 2023; 29: 833–845. https://doi.org/10.1038/s41591-023-02230-w.

[3] Lin Z, Li J, Zhang J, Feng W, Lu J, Ma X, *et al*. Metabolic Reprogramming Driven by IGF2BP3 Promotes Acquired Resistance to EGFR Inhibitors in Non-Small Cell Lung Cancer. Cancer Research. 2023; 83: 2187–2207. https://doi.org/10.1158/0008-5472.CAN-22-3059.

[4] Liu S, Zhang X, Wang W, Li X, Sun X, Zhao Y, *et al*. Metabolic reprogramming and therapeutic resistance in primary and metastatic breast cancer. Molecular Cancer. 2024; 23: 261. https://doi.org/10.1186/s12943-024-02165-x.

[5] Tiranti V, Viscomi C, Hildebrandt T, Di Meo I, Mineri R, Tiveron C, *et al*. Loss of ETHE1, a mitochondrial dioxygenase, causes fatal sulfide toxicity in ethylmalonic encephalopathy. Nature Medicine. 2009; 15: 200–205. https://doi.org/10.1038/nm.1907.

[6] Tiranti V, Briem E, Lamantea E, Mineri R, Papaleo E, De Gioia L, *et al*. ETHE1 mutations are specific to ethylmalonic encephalopathy. Journal of Medical Genetics. 2006; 43: 340–346. https://doi.org/10.1136/jmg.2005.036210.

[7] Kaur C, Mustafiz A, Sarkar AK, Ariyadasa TU, Singla-Pareek SL, Sopory SK. Expression of abiotic stress inducible ETHE1-like protein from rice is higher in roots and is regulated by calcium. Physiologia Plantarum. 2014; 152: 1–16. https://doi.org/10.1111/ppl.12147.

[8] Grings M, Seminotti B, Karunanidhi A, Ghaloul-Gonzalez L, Mohsen AW, Wipf P, *et al*. ETHE1 and MOCS1 deficiencies: Disruption of mitochondrial bioenergetics, dynamics, redox

homeostasis and endoplasmic reticulum-mitochondria crosstalk in patient fibroblasts. Scientific Reports. 2019; 9: 12651. https://doi.org/10.1038/s41598-019-49014-2.

[9] Tiranti V, D'Adamo P, Briem E, Ferrari G, Mineri R, Lamantea E, *et al*. Ethylmalonic encephalopathy is caused by mutations in ETHE1, a gene encoding a mitochondrial matrix protein. American Journal of Human Genetics. 2004; 74: 239–252. https://doi.org/10.1086/381653.

[10] Higashitsuji H, Higashitsuji H, Nagao T, Nonoguchi K, Fujii S, Itoh K, *et al*. A novel protein overexpressed in hepatoma accelerates export of NF-kappa B from the nucleus and inhibits p53-dependent apoptosis. Cancer Cell. 2002; 2: 335–346. https://doi.org/10.1016/s1535-6108(02)00152-6.

[11] Higashitsuji H, Higashitsuji H, Masuda T, Liu Y, Itoh K, Fujita J. Enhanced deacetylation of p53 by the anti-apoptotic protein HSCO in association with histone deacetylase 1. The Journal of Biological Chemistry. 2007; 282: 13716–13725. https://doi.org/10.1074/jbc.M609751200.

[12] Glaviano A, Foo ASC, Lam HY, Yap KCH, Jacot W, Jones RH, *et al*. PI3K/AKT/mTOR signaling transduction pathway and targeted therapies in cancer. Molecular Cancer. 2023; 22: 138. https://doi.org/10.1186/s12943-023-01827-6.

[13] He Y, Sun MM, Zhang GG, Yang J, Chen KS, Xu WW, *et al*. Targeting PI3K/Akt signal transduction for cancer therapy. Signal Transduction and Targeted Therapy. 2021; 6: 425. https://doi.org/10.1038/s41392-021-00828-5.

[14] Yu L, Wei J, Liu P. Attacking the PI3K/Akt/mTOR signaling pathway for targeted therapeutic treatment in human cancer. Seminars in Cancer Biology. 2022; 85: 69–94. https://doi.org/10.1016/j.semcancer.2021.06.019.

[15] Tantai J, Pan X, Chen Y, Shen Y, Ji C. TRIM46 activates AKT/HK2 signaling by modifying PHLPP2 ubiquitylation to promote glycolysis and chemoresistance of lung cancer cells. Cell Death & Disease. 2022; 13: 285. https://doi.org/10.1038/s41419-022-04727-7.

[16] Du X, Qi Z, Jiao Y, Wu W, Huang Q, Sun X, *et al*. HK2 promotes migration and invasion of intrahepatic cholangiocarcinoma via enhancing cancer stem-like cells' resistance to anoikis. Cellular Signalling. 2024; 118: 111126. https://doi.org/10.1016/j.cellsig.2024.111126.

[17] Jiao L, Zhang HL, Li DD, Yang KL, Tang J, Li X, *et al*. Regulation of glycolytic metabolism by autophagy in liver cancer involves selective autophagic degradation of HK2 (hexokinase 2). Autophagy. 2018; 14: 671–684. https://doi.org/10.1080/15548627.2017.1381804.

[18] Fontana F, Giannitti G, Marchesi S, Limonta P. The PI3K/Akt Pathway and Glucose Metabolism: A Dangerous Liaison in Cancer. International Journal of Biological Sciences. 2024; 20: 3113–3125. https://doi.org/10.7150/ijbs.89942.

[19] Liu Y, Fang C, Luo J, Gong C, Wang L, Zhu S. Traditional Chinese Medicine for Cancer Treatment. The American Journal of Chinese Medicine. 2024; 52: 583–604. https://doi.org/10.1142/S0192415X24500253.

[20] Yuan J, Liu Y, Zhang T, Zheng C, Ding X, Zhu C, *et al*. Traditional Chinese medicine for breast cancer treatment: a bibliometric and visualization analysis. Pharmaceutical Biology. 2024; 62: 499–512. https://doi.org/10.1080/13880209.2024.2359105.

[21] Wei J, Liu Z, He J, Liu Q, Lu Y, He S, *et al*. Traditional Chinese medicine reverses cancer multidrug resistance and its mechanism. Clinical & Translational Oncology: Official Publication of the Federation of Spanish Oncology Societies and of the National Cancer Institute of Mexico. 2022; 24: 471–482. https://doi.org/10.1007/s12094-021-02716-4.

[22] Cayetano-Salazar L, Olea-Flores M, Zuñiga-Eulogio MD, Weinstein-Oppenheimer C, Fernández-Tilapa G, Mendoza-Catalán MA, *et al*. Natural isoflavonoids in invasive cancer therapy: From bench to bedside. Phytotherapy Research: PTR. 2021; 35: 4092–4110. https://doi.org/10.1002/ptr.7072.

[23] Chen H, Fang C, Zhi X, Song S, Gu Y, Chen X, *et al*. Neobavaisoflavone inhibits osteoclastogenesis through blocking RANKL signalling-mediated TRAF6 and c-Src recruitment and NF-κB, MAPK and Akt pathways. Journal of Cellular and Molecular Medicine. 2020; 24: 9067–9084. https://doi.org/10.1111/jcmm.15543.

[24] Cai X, Zhou F, Xie X, Zheng D, Yao Y, Zhao C, *et al*. Neobavaisoflavone Demonstrates Valid Anti-tumor Effects in Non-Small- Cell Lung Cancer by Inhibiting STAT3. Combinatorial Chemistry & High Throughput Screening. 2022; 25: 29–37. https://doi.org/10.2174/1386207323666201204135941.

[25] Yuan Q, Wang J, Guo L, Xu Y, Hu L, Mao H, *et al*. Neobavaisoflavone ameliorates LPS-induced RAW264.7 cell inflammations by suppressing the activation of NF-κB and MAPKs signaling pathways. Iranian Journal of Basic Medical Sciences. 2022; 25: 1021–1027. https://doi.org/10.22038/IJBMS.2022.65372.14389.

[26] Don MJ, Lin LC, Chiou WF. Neobavaisoflavone stimulates osteogenesis via p38-mediated up-regulation of transcription factors and osteoid genes expression in MC3T3-E1 cells. Phytomedicine: International Journal of Phytotherapy and Phytopharmacology. 2012; 19: 551–561. https://doi.org/10.1016/j.phymed.2012.01.006.

[27] Ashrafi A, Akter Z, Modareszadeh P, Modareszadeh P, Berisha E, Alemi PS, *et al*. Current Landscape of Therapeutic Resistance in Lung Cancer and Promising Strategies to Overcome Resistance. Cancers. 2022; 14: 4562. https://doi.org/10.3390/cancers14194562.

[28] Kim YJ, Choi WI, Ko H, So Y, Kang KS, Kim I, *et al*. Neobavaisoflavone sensitizes apoptosis via the inhibition of metastasis in TRAIL-resistant human glioma U373MG cells. Life Sciences. 2014; 95: 101–107. https://doi.org/10.1016/j.lfs.2013.10.035.

[29] Maszczyk M, Banach K, Rok J, Rzepka Z, Beberok A, Wrześniok D. Evaluation of Possible Neobavaisoflavone Chemosensitizing Properties towards Doxorubicin and Etoposide in SW1783 Anaplastic Astrocytoma Cells. Cells. 2023; 12: 593. https://doi.org/10.3390/cells12040593.

[30] Li Y, Zhao R, Xiu Z, Yang X, Zhu Y, Han J, *et al*. Neobavaisoflavone induces pyroptosis of liver cancer cells via Tom20 sensing the activated ROS signal. Phytomedicine: International Journal of Phytotherapy and Phytopharmacology. 2023; 116: 154869. https://doi.org/10.1016/j.phymed.2023.154869.

[31] Maszczyk M, Rzepka Z, Rok J, Beberok A, Wrześniok D. Neobavaisoflavone May Modulate the Activity of Topoisomerase Inhibitors towards U-87 MG Cells: An In Vitro Study. Molecules (Basel, Switzerland). 2021; 26: 4516. https://doi.org/10.3390/molecules26154516.

[32] Hirai H, Sootome H, Nakatsuru Y, Miyama K, Taguchi S, Tsujioka K, *et al*. MK-2206, an allosteric Akt inhibitor, enhances antitumor efficacy by standard chemotherapeutic agents or molecular targeted drugs in vitro and in vivo. Molecular Cancer Therapeutics. 2010; 9: 1956–1967. https://doi.org/10.1158/1535-7163.MCT-09-1012.

[33] Sun D, Wang J, Zhang H, Liu S, Wei P, Wang H, *et al*. MK2206 Enhances Cisplatin-Induced Cytotoxicity and Apoptosis in Testicular Cancer Through Akt Signaling Pathway Inhibition. Translational Oncology. 2020; 13: 100769. https://doi.org/10.1016/j.tranon.2020.100769.

[34] Chen CYC. TCM Database@Taiwan: the world's largest traditional Chinese medicine database for drug screening in silico. PloS One. 2011; 6: e15939. https://doi.org/10.1371/journal.pone.0015939.

[35] Shi S, Tan P, Yan B, Gao R, Zhao J, Wang J, *et al*. ER stress and autophagy are involved in the apoptosis induced by cisplatin in human lung cancer cells. Oncology Reports. 2016; 35: 2606–2614. https://doi.org/10.3892/or.2016.4680.

[36] Smith TA. Mammalian hexokinases and their abnormal expression in cancer. British Journal of Biomedical Science. 2000; 57: 170–178.

[37] Thompson CB. Metabolic enzymes as oncogenes or tumor suppressors. The New England Journal of Medicine. 2009; 360: 813. https://doi.org/10.1056/NEJMe0810213.

[38] Herling A, König M, Bulik S, Holzhütter HG. Enzymatic features of the glucose metabolism in tumor cells. The FEBS Journal. 2011; 278: 2436–2459. https://doi.org/10.1111/j.1742-4658.2011.08174.x.

[39] Xia Y, Wang X, Liu Y, Shapiro E, Lepor H, Tang MS, *et al*. PKM2 Is Essential for Bladder Cancer Growth and Maintenance. Cancer Research. 2022; 82: 571–585. https://doi.org/10.1158/0008-5472.CAN-21-0403.

[40] Wu B, Liang Z, Lan H, Teng X, Wang C. The role of PKM2 in cancer progression and its structural and biological basis. Journal of Physiology and Biochemistry. 2024; 80: 261–275. https://doi.org/10.1007/s13105-024-01007-0.

[41] Colardo M, Segatto M, Di Bartolomeo S. Targeting RTK-PI3K-mTOR Axis in Gliomas: An Update. International Journal of Molecular Sciences. 2021; 22: 4899. https://doi.org/10.3390/ijms22094899.

[42] Dong CR, Hu DX, Liu SC, Luo HL, Zhang WJ. AKT/GSK-3beta/VEGF signaling is involved in P2RY2 activation-induced the proliferation and metastasis of gastric cancer. Carcinogenesis. 2023; 44: 65–79. https://doi.org/10.1093/carcin/bgac095.

[43] da Silva MF, Lins AA, Gomes MC, de Jesus Marinho WP, de Araujo RSA, de Moura RO, *et al*. Anticancer Drug Discovery from Natural Compounds Targeting PI3K/AKT/mTOR Signaling Pathway. Current Medicinal Chemistry. 2025; 32: 4859–4887. https://doi.org/10.2174/0109298673325229240928040758.

[44] Huang M, Lu JJ, Ding J. Natural Products in Cancer Therapy: Past, Present and Future. Natural Products and Bioprospecting. 2021; 11: 5–13. https://doi.org/10.1007/s13659-020-00293-7.

[45] Ying Q, Fan R, Shen Y, Chen B, Zhang J, Li Q, *et al*. Small Cell Lung Cancer-An Update on Chemotherapy Resistance. Current Treatment Options in Oncology. 2024; 25: 1112–1123. https://doi.org/10.1007/s11864-024-01245-w.

[46] Cunha A, Silva PMA, Sarmento B, Queirós O. Targeting Glucose Metabolism in Cancer Cells as an Approach to Overcoming Drug Resistance. Pharmaceutics. 2023; 15: 2610. https://doi.org/10.3390/pharmaceutics15112610.